Deltares

Ten Noorden van de Waddeneilanden Field Measurement Campaign

Validation Report - September 2019

Deltares

Ten Noorden van de Waddeneilanden Field Measurement Campaign

Validation Report - September 2019

Sofia Caires

11203488

Deltares

Title
Ten Noorden van de Waddeneilanden Field Measurement Campaign

Client	Project	Reference	Pages
Fugro	11203488	11203488-002-HYE-0002	63

Classification
None

Keywords
North Sea, wind farm, metocean data, validation, offshore wind

Summary

Two *SEAWATCH Wind LiDAR Buoys*, TNWA and TNWB, and a bottom mounted sensor associated to TNWB have been deployed by Fugro at the Ten Noorden van de Waddeneilanden Wind Farm Zone on the 19th of June 2019, with the intention of measuring wind, waves, temperatures, pressures and currents for a period of two years. This report focuses on the validation of the measurements during September 2019.

The validation is performed by comparing the TNWA and TNWB observations against each other and with wind, waves, air and water temperature, air pressure and currents from a variety of reliable sources (anemometer, LiDAR, hydrodynamic model, etc) at reference stations in the North Sea; namely L91, F161, K13, F3, AWG, HG, SON and BG.

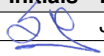The following conclusions ensue from the validation of the data.

- The comparisons between the TNWA and TNWB wind velocities show at all levels and in terms of both wind speed and direction low biases and correlations and slopes close to 1, indicating correct functioning of both LiDARs. Furthermore, there is a poor to reasonable (reasonable to excellent) agreement between the wind speed (direction) observations from TNW and those from the fixed platforms. The found mismatches can be explained by local effects and spatial variations.
- The agreement between the TNWA and TNWB wave parameters is excellent for all parameters, except in terms of peak wave period which is good and mean wave direction of swell which is poor. The poorer agreements are as expected, given that these parameters depend more strongly on the sampling variability (randomness of the sea surface elevation) and discreteness of the wave spectra. The agreement between the wave observations from TNW and from the reference stations is relatively high, especially when considering local refraction and the distances between the stations.
- The validation of the temperature data shows that there is a general agreement between TNW temperature observations and those from nearby stations.
- The validation of the air pressure data shows, as expected given their proximity in terms of macro-atmospheric forcings, an excellent agreement between the TNW observations and those from the fixed stations.
- The agreement between the current speed observations and model results is high. There are mismatches between the current directions, which are partly due to the nature and variability of the current direction signal.

The availability of the buoy data is high for all variables except for the LiDAR wind data which is poor, with no data available from the LiDAR at TNWB from 00:10 on the 12th of September, when connection with the LiDAR was lost, and many gaps in the TNWA data.

The overall conclusion of the validation is that this TNWA and TNWB dataset is of high quality and trustworthy.

References

None

Version	Date	Author	Initials	Review	Initials	Approval	Initials
1.0	Nov 27, 2019	S. Caires		J. Schouten		M. van Gent	

Status

Final

Contents

Deltares

List of Figures

Deltares

List of Tables

Deltares

1 Introduction

Aiming at high collection rates of quality metocean data, two *SEAWATCH Wind LiDAR Buoys* were deployed by Fugro at the Ten Noorden van de Waddeneilanden Wind Farm Zone. The two buoys are referred to as Station A and Station B but are abbreviated in this report as TNWA and TNWB, respectively. Additionally, a bottom mounted water level sensor (WLS) has been deployed near the TNWB buoy[1]. The deployment date is the 19th of June 2019. The campaign aims at measuring wind, waves, temperatures, pressures and currents for a period of two years and the redundant arrangement of instruments is intended to safeguard against loss in measured data.

Information regarding the locations of the buoys is given in Table 1.1. The WLS have been deployed close to the TNWB buoy mooring locations and its coordinates are assumed to coincide with those of the buoy. The bathymetry around the approximate location of the buoys is shown in Figure 1.1.

Table 1.1: *Ten Noorden van de Waddeneilanden LiDAR Buoy mooring locations.*

Station	S.no.	Longitude (E)	Latitude (N)	Depth (mMSL)
TNWA	WS190	5.5502°	54.0181°	≈ 38
TNWB	WS191	5.5498°	54.0218°	≈ 38
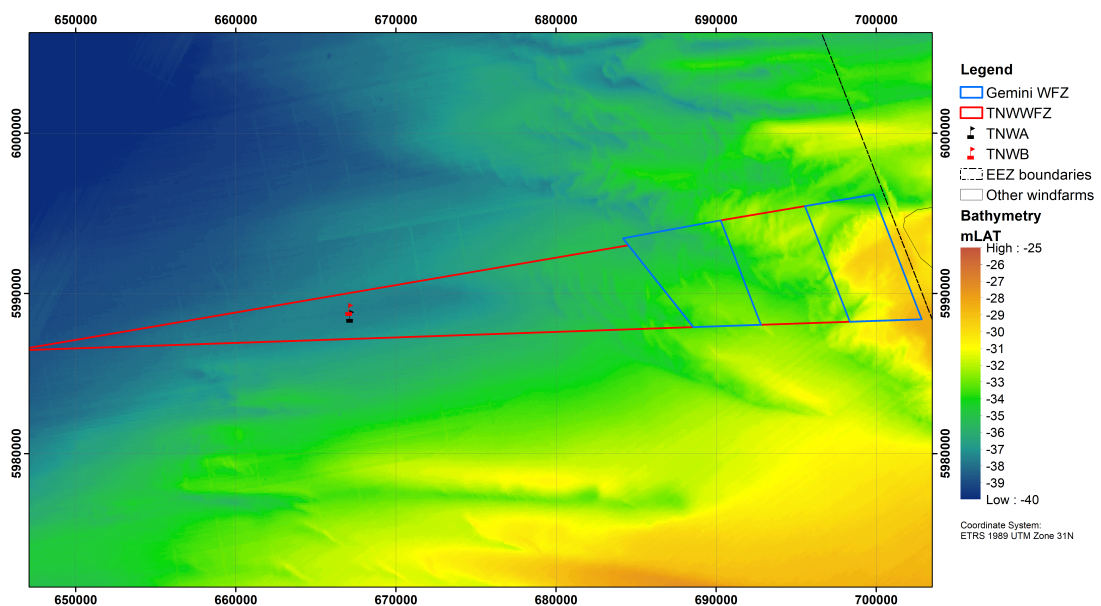
Figure 1.1: *Bathymetry (mLAT, mLAT$\approx$ -1 mMSL) around the buoy locations.*

The main aim of this report it to provide an overview and validation of the TNW post-processed wind, wave, temperature, air pressure and current observations, mainly focusing on the validation of the wind, wave and current data. The assessment of the integrity of the buoy data processing and the quality of the pre-processed data are outside the scope of the validation. The validation is carried out by quantifying the agreement

---

[1]A WLS was also deployed near the TNWA buoy but it failed right after deployment.

between the TNWA and TNWB data, indicating correct functioning of the different sensors without loss of accuracy, and data from other reliable sources (anemometer, LiDAR, atmospheric model, hydrodynamic model, etc) at fixed North Sea reference stations (no temporary campaigns). If the same variations are found in the parameters, this can be seen as an indication that both buoy systems are functioning correctly with no system errors in the measurements. Furthermore, for some variables their general characteristics are also qualitatively assessed, such as for current and wind measurements their respective vertical profiles. Per variable the most suitable available data validation sources have been sought, leading to the following combinations:

- The reference stations for validating the buoy wind data against anemometer observations are those from platform L91 (where the anemometer is at height z=87m), referred to as L91, platform F161 (z=75.5m), referred to as F161, platform K13 (z=73.8), referred to as K13, platform F3 (z=60m), referred to as F3, platform Ameland Westgat (z=60m), referred to as AWG and those from the Huibergat station (z=18m), referred to as HG. These stations are approximately at a distance of respectively 59 km (L91), 101 km (F161), 178 km (K13), 107 km (F3), 64 km (AWG) and 75 km (HG) from the TNW buoys. F161, K13 and F3 are thus at a considerable distance from TNWA and TNWB and the comparisons between these data can be expected to be poor. These data are still considered to provide a measure of spatial variability. The considered anemometer observations, as most other observations considered in this study, have been collected by the Dutch Government (see http://matroos.rws.nl/). LiDAR wind velocity observations at vertical levels 63 m, 91 m, 116 m, 141 m, 166 m, 191 m and 241 at K13 from the Energy research Centre of the Netherlands (ECN) part of the Dutch organization for applied research (TNO) have also been made available and are also considered in the validation of the wind data. Furthermore, winds at 10 m height from the Dutch Meteorological Institute (KNMI) operational Numerical Weather Prediction model Hirlam7.2 (KNMI, 2009) are also considered in the evaluation of the spatial variations.
- The wave heights, periods and directions are also validated against Dutch Government observations. The locations for validating the buoy wave data are F161, F3 and Schiermonnikoog Noord, referred to as SON and at about 62 km from the TNW buoys.
- The Dutch Government observations at K13 and SON are used for validating the water temperature.
- Available online data (https://mesonet.agron.iastate.edu/request/download.phtml?network=NL__ASOS) from weather stations located at Buitengats, referred to as BG and located within the TNW region, are used for validating the air temperature.
- Dutch Government observations at K13, F3, F161 and L91 are used for validating air pressure.
- Lastly, given the lack of fixed observation sources, the currents are validated against predictions from a purposely run by Deltares 3D hydrodynamic model.

Figure 1.2 shows an overview of all measurement locations. The present report provides the validation results for the period - 'September 2019' - extending from September 01 00:00 to September 30 23:50.

Deltares
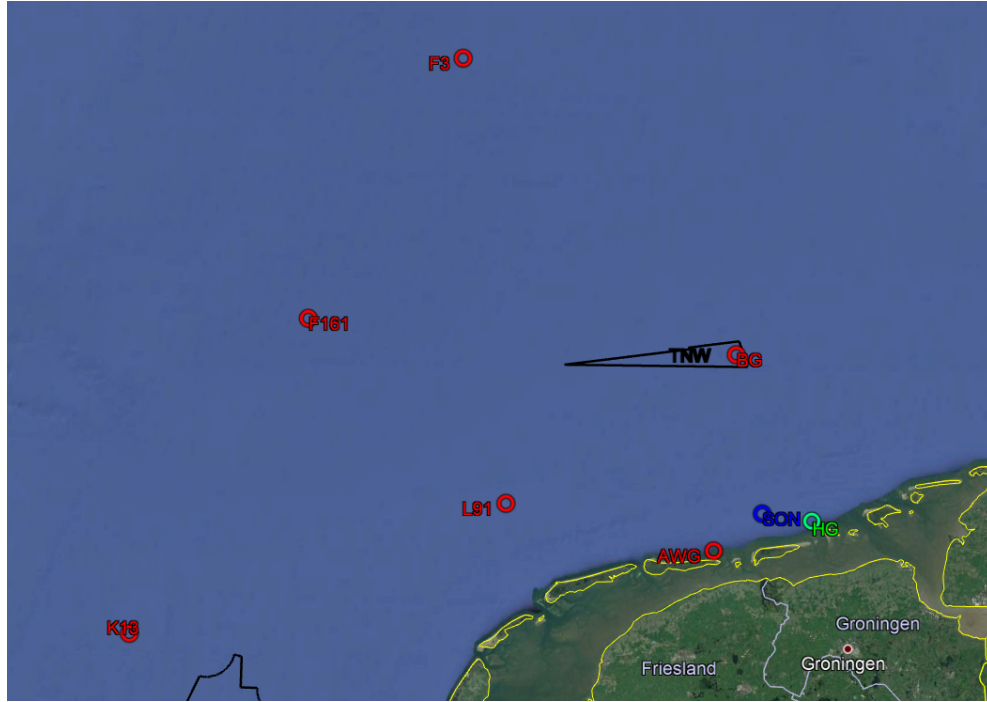
Figure 1.2: *Aerial view of the location of the buoys and fixed measurement stations (via Google Earth).*

All comparisons are presented as a timeseries and further validated via direct scatter plots for quantifying statistical correspondence between the datasets.

The error statistics are computed differently whether a linear or circular (directional) variable is considered. For linear variables we have:

- the bias: $\bar{y} - \bar{x}$;
- the root-mean-square error: rmse = $\sqrt{n^{-1} \sum (y_i - x_i)^2}$;
- the symmetric slope: s = $\sqrt{\sum x_i{}^2 / \sum y_i{}^2}$; and
- the correlation coefficient:

$$r = \sum \left[(x_i - \bar{x})(y_i - \bar{y}) \right] / \sqrt{\sum (x_i - \bar{x})^2 \sum (y_i - \bar{y})^2} \ .$$

In all these formulae x_i usually represents observations (or the dataset which is considered less uncertain or baseline) and in this study we use it to represent the fixed observations, y_i usually represents the model results (or the dataset which is considered more uncertain or with a certain deviation from the baseline results) and in this study we use it to represent the TNWA and TNWB data and n the number of observations.

When dealing with circular data, each observation is considered as unit vector, and it requires vector addition rather than ordinary (or scalar) addition to compute the average of angles, the so-called mean direction.

Writing

$$C_n = \sum_{i=1}^{n} \cos x_i \quad and \quad S_n = \sum_{i=1}^{n} \sin x_i, \tag{1.1}$$

the sample resultant vector R_n of a sample $\mathbf{x} = x_i,\ i = 1, ..., n$ is defined as $R_n = \sqrt{C_n^2 + S_n^2}$, and its sample mean direction $\bar{x} \equiv \bar{x}_n$ as the direction of R_n:

$$\bar{x} = TAN^{-1}(S_n/C_n)$$

where

$$TAN^{-1}(S_n/C_n)$$

is the inverse of the tangent of

$$(S_n/C_n)$$

in the range $[0, 2\pi]$, i.e.,

$$TAN^{-1}(S_n/C_n) := \begin{cases} \tan^{-1}(S_n/C_n), & S_n > 0, \ \ C_n > 0 \\ \tan^{-1}(S_n/C_n) + \pi, & C_n < 0 \\ \tan^{-1}(S_n/C_n) + 2\pi, & S_n < 0, \ \ C_n > 0. \end{cases} \tag{1.2}$$

The sample mean resultant length of $\mathbf{x} = x_i,\ i = 1, ..., n$ is defined by $\bar{R}_n = R_n/n$, $0 \le \bar{R}_n \le 1$. If $\bar{R}_n = 1$, then all angles coincide.

Equation 1.2 can be used to compute the bias between two circular variables by substituting x_i by $y_i - x_i$ in Equation 1.1. In a similar way, the root-mean-square error between two circular variables can be computed.

There are several circular analogues of the correlation coefficient, but the most widely used is the so-called T-linear correlation coefficient (Fisher and Lee (1983) and Fisher (1993)). Given two sets $\mathbf{x} = x_i,\ i = 1, ..., n, \mathbf{y} = y_i,\ i = 1, ..., n$ of circular data, the T-linear correlation coefficient between x and y is defined by

$$r = \frac{\sum\limits_{1 \le i < j \le n} \sin(x_i - x_j)\sin(y_i - y_j)}{\sqrt{\sum\limits_{1 \le i < j \le n} \sin^2(x_i - x_j) \sum\limits_{1 \le i < j \le n} \sin^2(y_i - y_j)}}. \tag{1.3}$$

In the following we shall refer to comparisons in which r is higher than 0.9 as excellent, between 0.8 and 0.9 as good, between 0.7 and 0.8 as reasonable and lower than 0.7 as poor. Note that this is no absolute quality statement given that there are uncertainties in both observations and, due to the distance between the instruments, the spatial variability is expected to affect the comparisons.

Note that all reported dates are in GMT (which is equivalent to UTC).

2 Data Availability

Although in measuring campaigns the aim is always of having a full (gap free) timeseries of all measured parameters, they are typically hampered by severe metocean conditions and loss of signal between instruments. Figure 2.1 shows a detailed breakdown for each buoy of the amount of missing data throughout the temporal record for each measured parameter. The availability of the data is computed from September 01 00:00 to September 30 23:50. Note that in this validation study only processed data (10 minute averages in the case of wind) are considered. The original raw observations have been processed and quality checked by Fugro. Furthermore, data from all processed variables are supposed to be available every 10 minutes (at the hour and 10, 20 30, 40 and 50 minutes after the hour). Table 2.1 gives a brief explanation of what the variable names in Figure 2.1 mean, their units and, if applicable, the symbols used to refer to them.

As can be seen in Figure 2.1, the collected data consists of wind speed and direction at different heights, a number of wave height, period and direction parameters, current speed and direction at different depths, water and air temperature, pressure and humidity.

We use the following qualification of data availability:

- >95% referred to as high availability,
- 90 - 95% referred to as good availability,
- 80 - 90% referred to as acceptable availability,
- 60 - 80% referred to as limited availability, and
- <60% referred to as poor availability.

The availability of the buoy data is high for all variables except for the LiDAR wind data which is poor, with no data available from the LiDAR at TNWB from 00:10 on the 12th of September, when connection was lost, and many gaps in the TNWA data. The availability of the bottom temperature data from the WLS is good.

Not all data being measured are considered in this report:

- Although the availability of the humidity data is given in Figure 2.1, the data are not considered further.
- The WLS is also recording the water pressure, but these data are also not being considered, at least for the time being. After the collection of six months of water pressure data Fugro will check whether the data can be used to infer water levels.
- The buoys are also recording the wave spectra, but it is not transmitted on an ongoing basis. They will only be available every 6 months or so, after service visits when all data are downloaded.
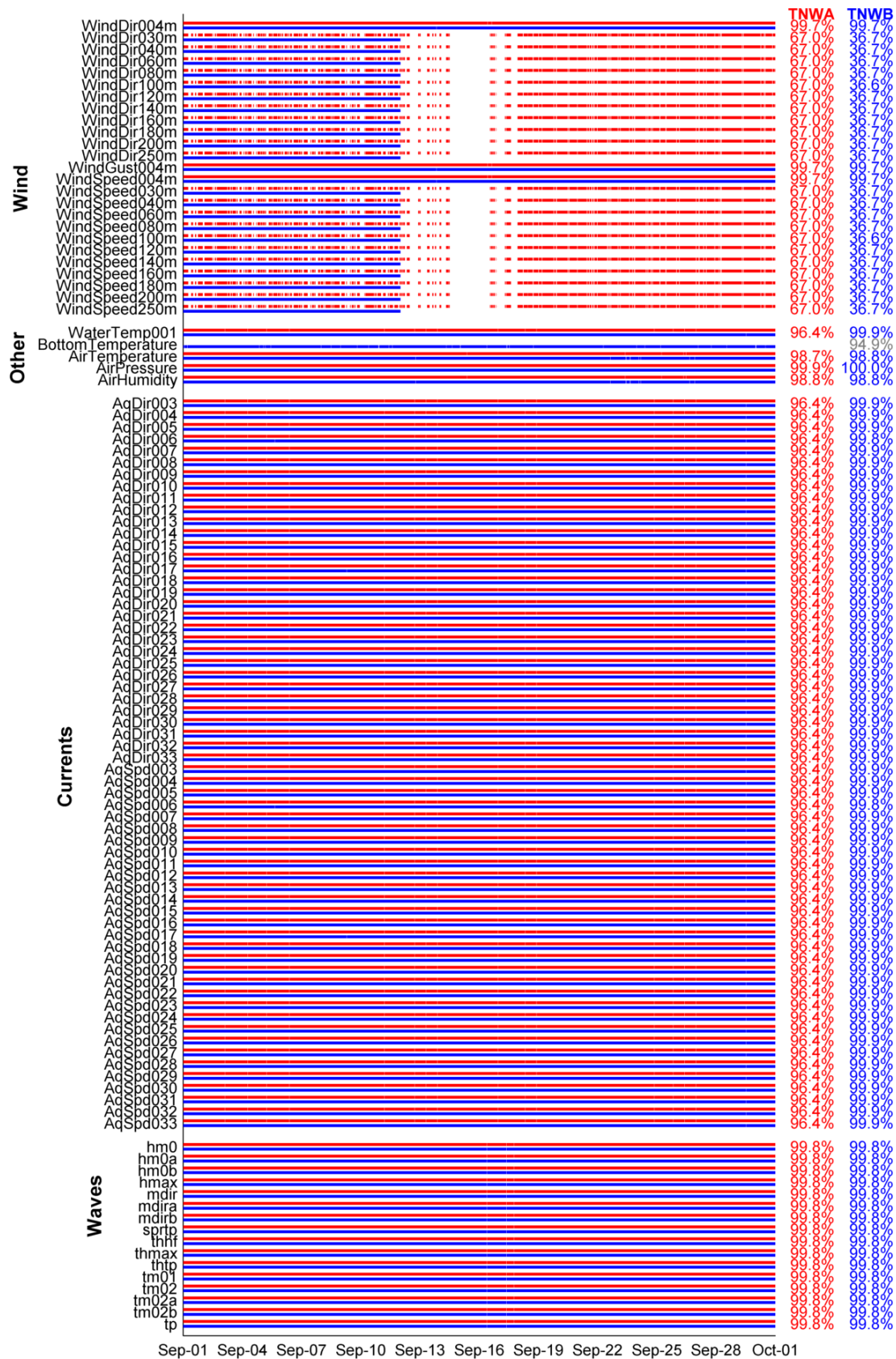
Figure 2.1: *Availability of the 10 minute TNWA (red), TNWB (blue) and WLS (grey) data of September 2019.*

Table 2.1: List of variables.

Name	Description	Units	Symbol
WindSpeed z mh	Wind speed at an elevation of z m above the sea surface	m/s	U_z
WindGust z mh	Wind gust speed at an elevation of z m above the sea surface	m/s	
WindDir z m	Wind direction at an elevation of z m above the sea surface	°N	$U_{z\theta}$
airTemperature	Air temperature	°C	T_{air}
airPressure	Air pressure	hPa	
airHumidity	Air humidity	%	
WaterTemp0001	Water temperature (surface)	°C	T_{water}
BottomTemp	Water temperature (bottom)	°C	T_{water}
AqSpd d	Current speed at a depth of d m below the sea surface	m/s	u_d
AqDir d	Current direction at a depth of d m below the sea surface	°N	
hm0	Spectral significant wave height	m	H_s
hm0a	Spectral significant swell wave height. Frequency band between 0.04 and 0.10 Hz.	m	H_{sswell}
hm0b	Spectral significant sea wave height. Frequency band between 0.10 and 0.50 Hz.	m	H_{ssea}
hmax	Spectral maximal individual wave height	m	H_{max}
mdir	Mean wave direction	°N	MWD
mdira	Mean wave direction of swell	°N	MWD_{swell}
mdirb	Mean wave direction of sea	°N	MWD_{sea}
sprtp	Wave spreading at spectral peak period	°	$DSPR$
thhf	High frequency mean wave direction. Frequency band between 0.4 and 0.44 Hz.	°N	
thmax	Period of highest wave.	s	
thtp	Wave direction at spectral peak period.	°N	
tm0x	Spectral mean absolute wave period (1 based on the 1st spectral moment, 2 based on the 2nd spectral moment, a swell, b sea)	s	T_{m0x}
tp	Spectral peak wave period	s	T_p

3 Wind

This chapter focuses on the validation of the wind velocity observations from the *SEAWATCH LiDAR Buoys*. The wind speed and direction are measured at 4 m above water level by a Sonic wind sensor and at levels 30, 40, 60, 80, 100, 120, 140, 160, 180, 200 and 250 m above water level by a LiDAR.

3.1 Ten Noorden van de Waddeneilanden description and intercomparison

To get a full overview of the data two movies are created with the time evolution of vertical wind profiles at TNWA (see here) and at TNWB (see here).

Given that for low wind speeds there is much scatter in the data and that these data are not relevant in the data analyses (profiles and error statistics), all observations for which the observed wind speeds are below 5 m/s are excluded. This threshold was chosen pragmatically, being in line with the work of Wieringa and Rijkoort (1983) and in line with other wind climate assessments of the Dutch meteorological institute and close to the 4 m/s threshold prescribed for the calibration of cup anemometers in the IEC 61400-12-1 standard.

Figure 3.1 provides an overview of the observed LiDAR data without the filtered low observations. The figure shows all observed vertical profiles for which the wind speed is above 5 m/s (grey lines), the mean profile (red line) and a fitted power profile (blue line).

The power law profile is described by:

$$U(z) = U_{30}\Big(\frac{z}{30}\Big)^{\alpha}$$

where U_{30} is the wind speed at 30m above the surface and α is the power-law constant. The fit given in Figure 3.1 has been obtained using least squares.

Figure 3.1 shows that the power law profile deviates slightly from the observed vertical wind profile, showing a slightly higher increase with height up to a height of about 60 m and an almost perfect match after that height.
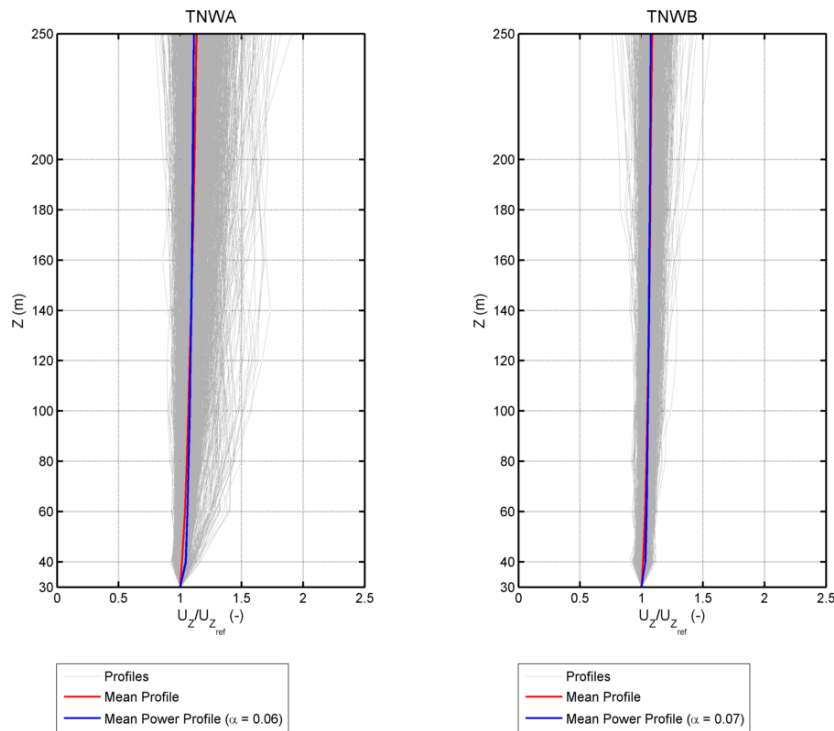
Figure 3.1: Normalized LiDAR wind speed vertical profiles (data from September 2019).

Figure 3.2 and Figure 3.3 show the timeseries of respectively the wind speed and direction at the observation levels. Only the data from the wind sensor are available during the whole period, with the stronger winds peaking close to 15 m/s at the sensor height. During most of the month the winds are from the Southwest-Northwest, with only short periods with the wind blowing from the East-Southeast, more predominantly between the 9th, 21st and 22nd of September. The available LiDAR observations are at all levels below 22 m/s.
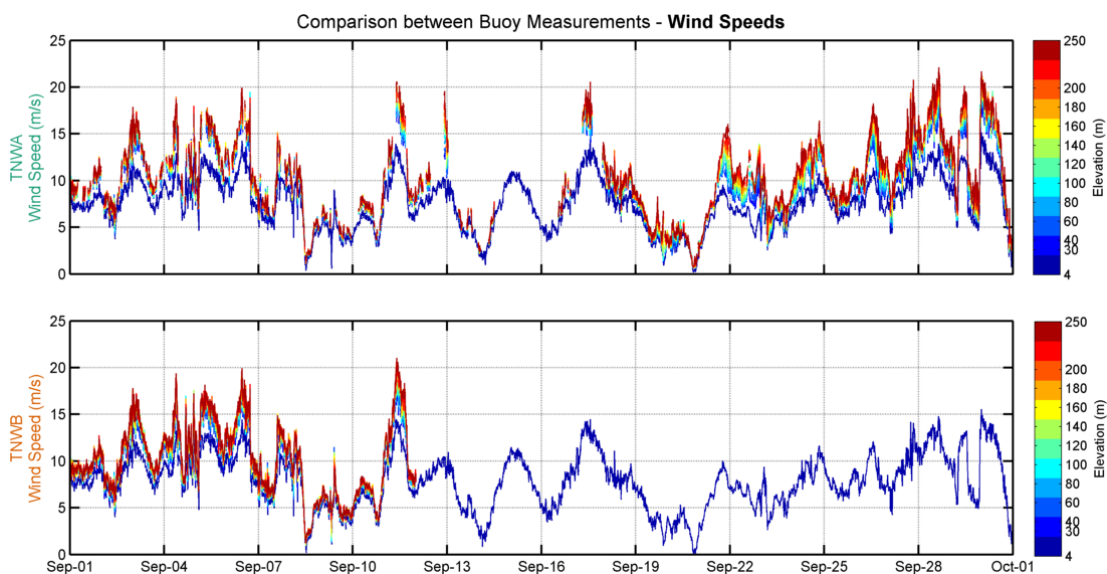
Figure 3.2: Wind speeds (by elevation) at each buoy.
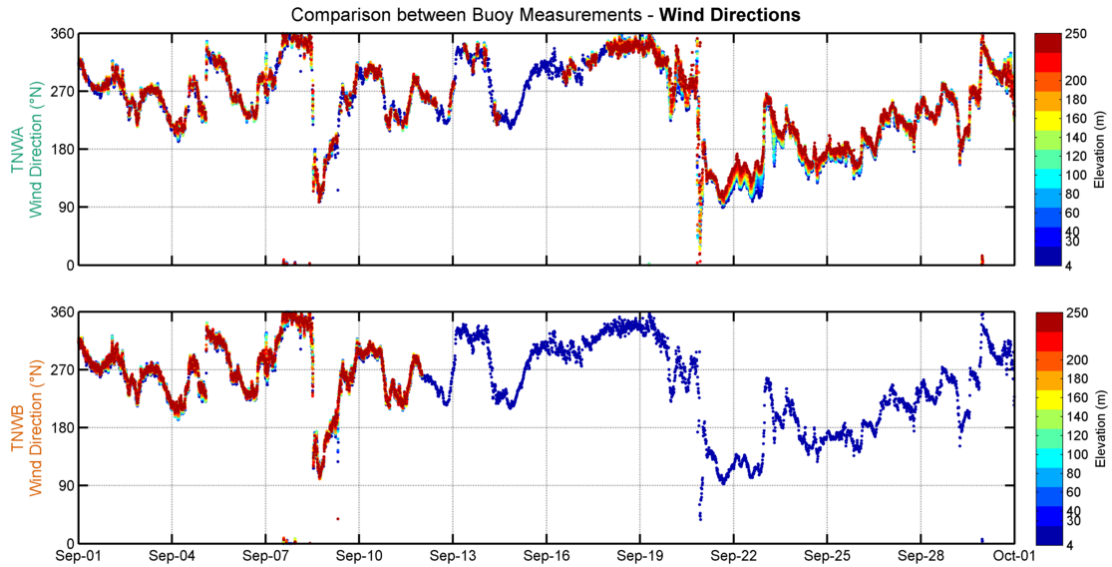
Figure 3.3: *Wind directions (by elevation) at each buoy.*

Figure 3.4 shows density scatter comparisons between the wind speed and direction measured by TNWA and TNWB at two chosen levels, 100m and 160m. The figure shows a general agreement between the observation of TNWA and TNWB, as could already be seen in figures 3.2 and 3.3.
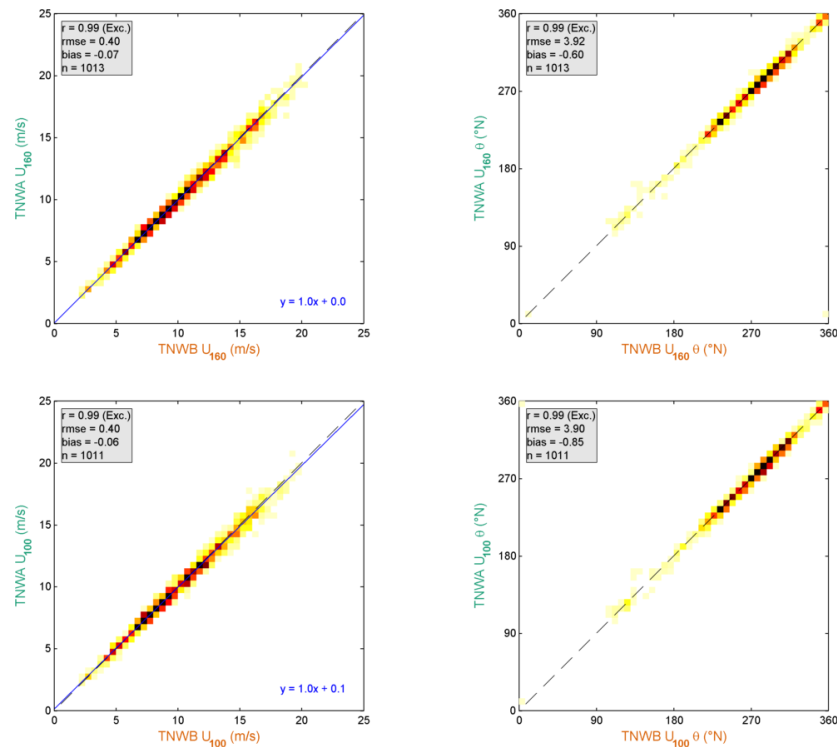
Figure 3.4: *Direct scatter comparison between LiDAR wind at 100 and 160 m (data from September 2019).*

In order to further quantify the differences between the TNWA and TNWB wind speed and direction observations, the slope, bias, correlations and square correlations between the TNWA and TNWB wind speed observations at all levels and the bias, correlations and

square correlations between the TNWA and TNWB wind direction observations at all levels have been computed considering all wind speeds above 2 m/s. These are given in Table 3.1 and (given the lower threshold) can be compared against the criteria given in IEC 61400-12-1 (2017) and IEA Wind (2017)[1]. The table shows that, even applying such a low wind speed threshold, the comparisons are at all levels excellent both in terms of wind speed and direction. Note that the obtained KPIs and are in line those obtained during the pre-validation of the LiDARs; in particular the squared correlations were between 0.97 and 0.99 for wind speed and 0.99 and 1 for wind direction, see DNV-GL (2019a) and DNV-GL (2019b).

Table 3.1: *Statistical comparison between the winds from the LiDAR buoys with elevation.*

Elev. (m)	Wind Speed					Wind Direction			
	r^2 (-)	r (-)	Bias (m/s)	Sym. Slope (-)	n (-)	r^2 (-)	r (-)	Bias (°N)	n (-)
4	0.98	0.99	0.30	1.04	4191	0.99	1.00	-1.6	4191
30	0.98	0.99	-0.07	0.99	1011	0.99	0.99	-0.9	1011
40	0.99	0.99	-0.06	0.99	1012	0.99	0.99	-0.7	1012
60	0.98	0.99	-0.07	0.99	1011	0.99	0.99	-0.9	1011
80	0.99	0.99	-0.07	0.99	1012	0.99	0.99	-0.9	1012
100	0.99	0.99	-0.06	0.99	1011	0.99	0.99	-0.8	1011
120	0.99	0.99	-0.04	1.00	1012	0.99	0.99	-0.8	1012
140	0.99	0.99	-0.05	0.99	1013	0.99	0.99	-0.7	1013
160	0.99	0.99	-0.07	0.99	1013	0.99	0.99	-0.6	1013
180	0.99	1.00	-0.05	0.99	1014	0.99	0.99	-0.7	1014
200	0.99	0.99	-0.07	0.99	1013	0.99	0.99	-0.8	1013
250	0.99	1.00	-0.05	0.99	1015	0.99	0.99	-0.9	1015

3.2 Validation

In this section the TNWA (Section 3.2.2) and TNWB (Section 3.2.3) wind data are validated against anemometer observations at L91 (at a height of z=87m and at a distance of about d= 59km from TNW), F161 (z=75.5m, d=101km), K13 (z=73.8m, d=178km), F3 (z=60m, d=107km), AWG (z=60m, d=64km), and HG (z=18m, d=75km). The wind speeds at several levels are validated against ECN LiDAR observations at K13 (z=63, 91, 116, 141, 166 and 191m). Note that F161, K13 and F3 are at a considerable distance from TNWA and TNWB and in periods with large spatial wind variations comparisons between these data can be expected to be poor. Furthermore, given its proximity to the coast, the winds blowing from the coast at HG and AWG are expected to be more strongly influenced by land effects. Nevertheless, data from these stations are still expected to show some correspondence with the TNW data and in any case to provide a measure of spatial variability and also variability in height.

An overview of the comparisons is first presented between the TNWA and TNWB buoys and the fixed platform anemometer datasets, followed by a comparison of each TNWA and TNWB buoys with measured fixed platform anemometer and LiDAR data.

3.2.1 Overview

Figure 3.5 provides an overview of the comparisons, comparing the timeseries of the L91, F161, K13, F3, AWG, and HG observations and the TNWA and TNWB LiDAR observations at the levels closer to those of the anemometers. A further overview of the comparisons

---

[1]Note that the applied T-linear correlation coefficient Equation 1.3 leads in general to slightly lower correlations between directions than those using the standard correlation as in the cited criteria.

Ten Noorden van de Waddeneilanden Field Measurement Campaign

between data at the buoy and platform locations is given by means of wind roses at Figure 3.6. The roses show a general alignment between the datasets, with the southeastern winds that occurred in the period with no data from the LiDAR at TNWB, clearly missing from the TNWB roses.
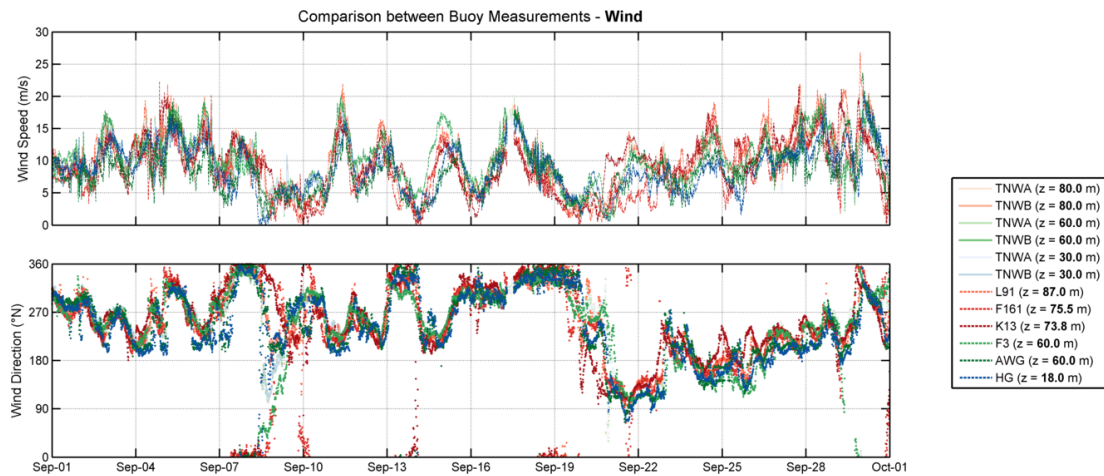
Figure 3.5: *Wind speed and direction for all locations (data from September 2019).*
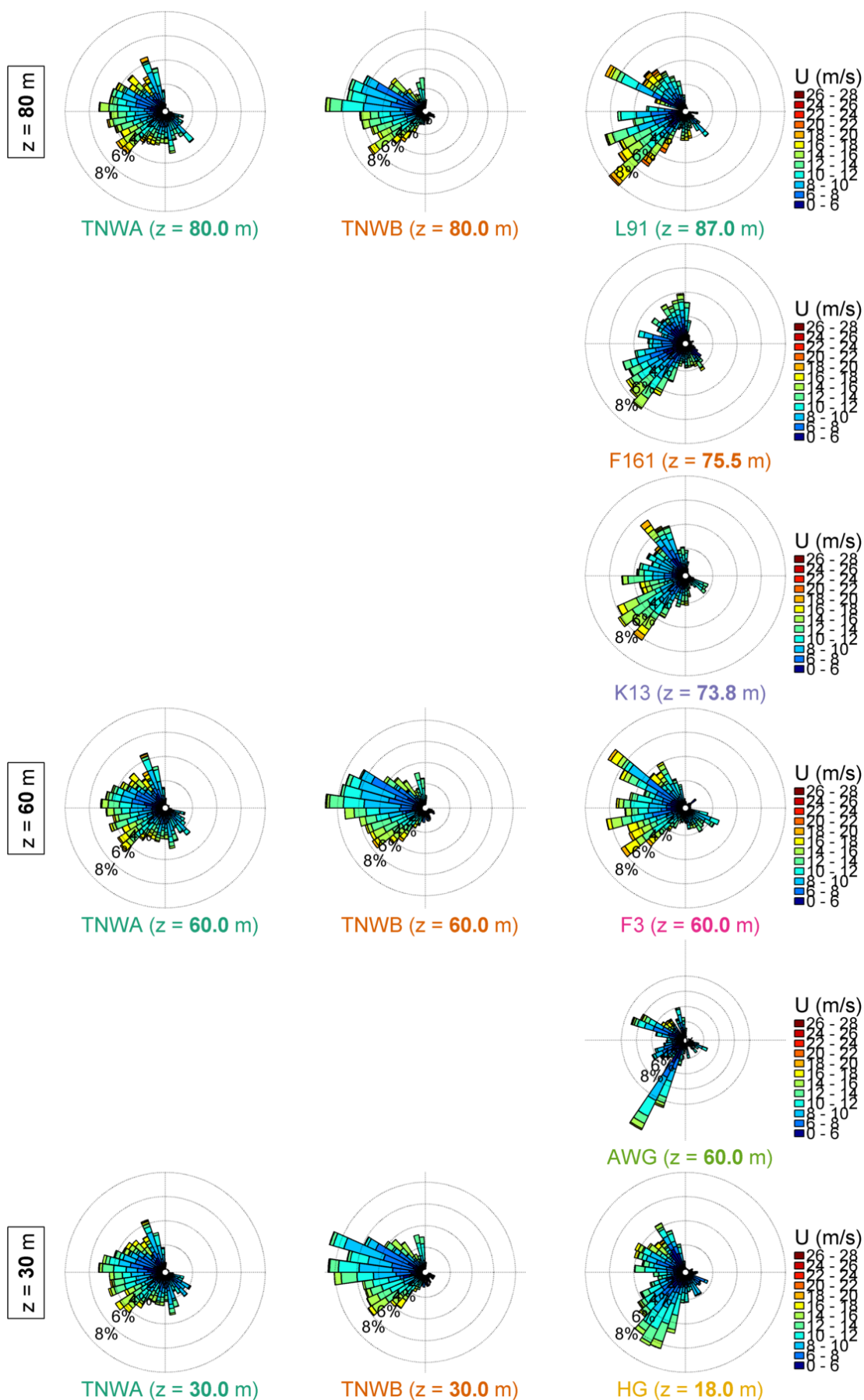
Figure 3.6: *Wind roses (of bin width 8°) for all locations (data from September 2019).*

3.2.2 Ten Noorden van de Waddeneilanden Buoy TNWA

3.2.2.1 Anemometer

Figure 3.7, Figure 3.8, Figure 3.9, Figure 3.10, Figure 3.11 and Figure 3.12 show comparisons between TNWA observations and those at L91, F161, K13, F3, AWG, and HG, respectively. The correlation, root-mean-square error and bias statistics are printed in the figures.

As can be seen in the figures, the comparisons between the TNWA observations and those from:

- L91 are reasonable in terms of wind speed and excellent in terms of wind direction,
- F161 are poor in terms of wind speed and good in terms of wind direction,
- K13 are poor in terms of wind speed and reasonable in terms of wind direction,
- F3 are reasonable in terms of wind speed and good in terms of wind direction, and
- AWG and HG are reasonable in terms of wind speed and good in terms of wind direction.

The low wind speed correlations are most likely due to the distance between the stations and the large spatial wind speed variations that generally occur when speeds are predominantly below 15 m/s as is the case in this period. As wind direction is less variable on shorter distances, statistical parameters on wind direction will in general show better comparison.

Figure 3.7: *Validation of TNWA (data from September 2019) with L19 wind data. Left panel: Timeseries. Middle panel: Density scatter, with the darker colours indicating more data density.*
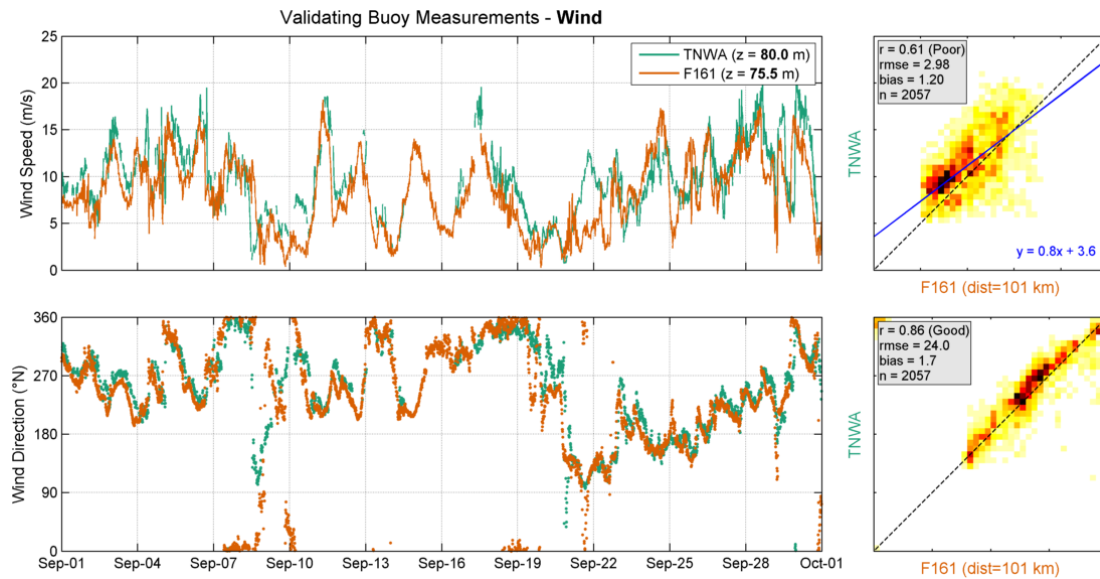
Figure 3.8: Validation of TNWA (data from September 2019) with F161 wind data. Left panel: Timeseries. Middle panel: Density scatter, with the darker colours indicating more data density.
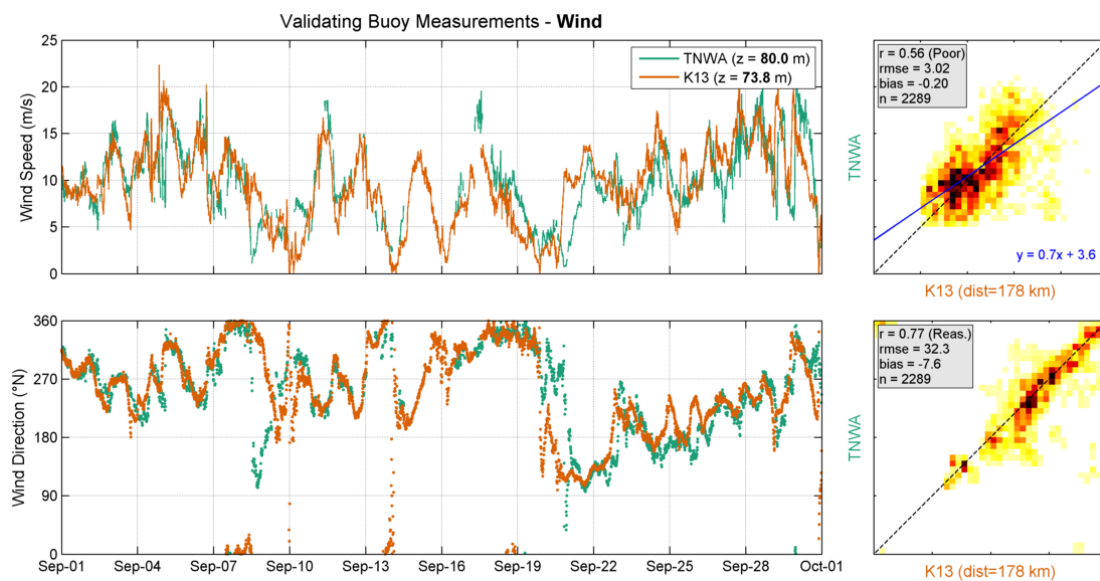
Figure 3.9: Validation of TNWA (data from September 2019) with K13 wind data. Left panel: Timeseries. Middle panel: Density scatter, with the darker colours indicating more data density.
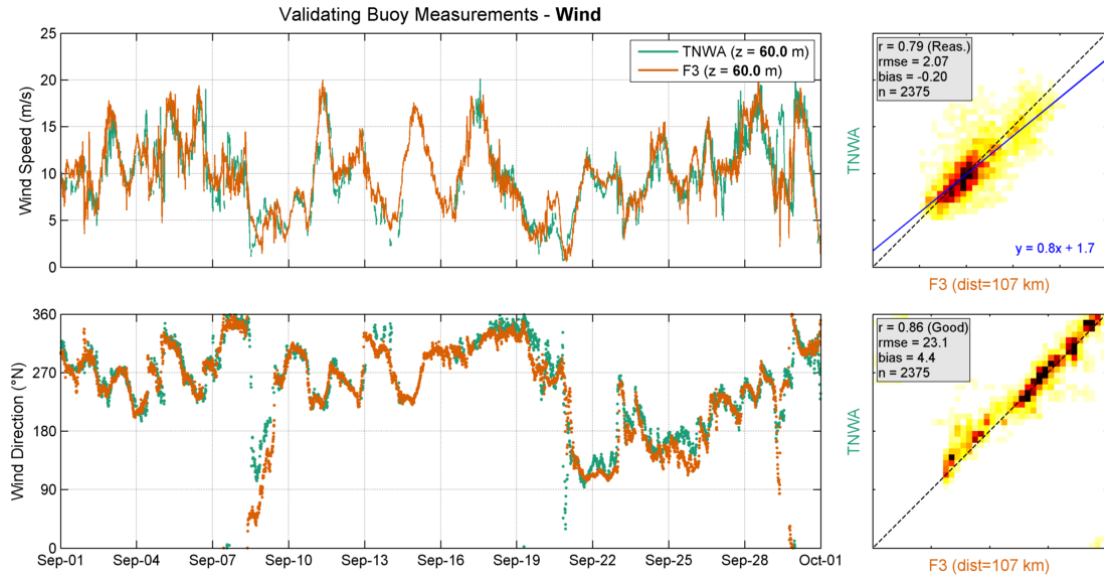
Figure 3.10: *Validation of TNWA (data from September 2019) with F3 wind data. Left panel: Timeseries. Middle panel: Density scatter, with the darker colours indicating more data density.*
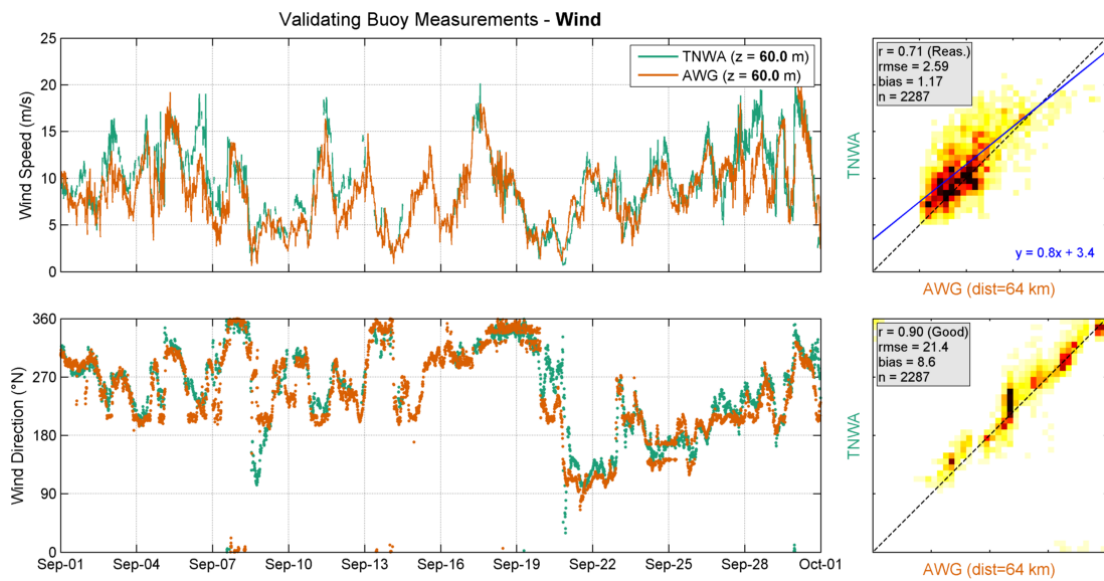
Figure 3.11: *Validation of TNWA (data from September 2019) with AWG wind data. Left panel: Timeseries. Middle panel: Density scatter, with the darker colours indicating more data density.*
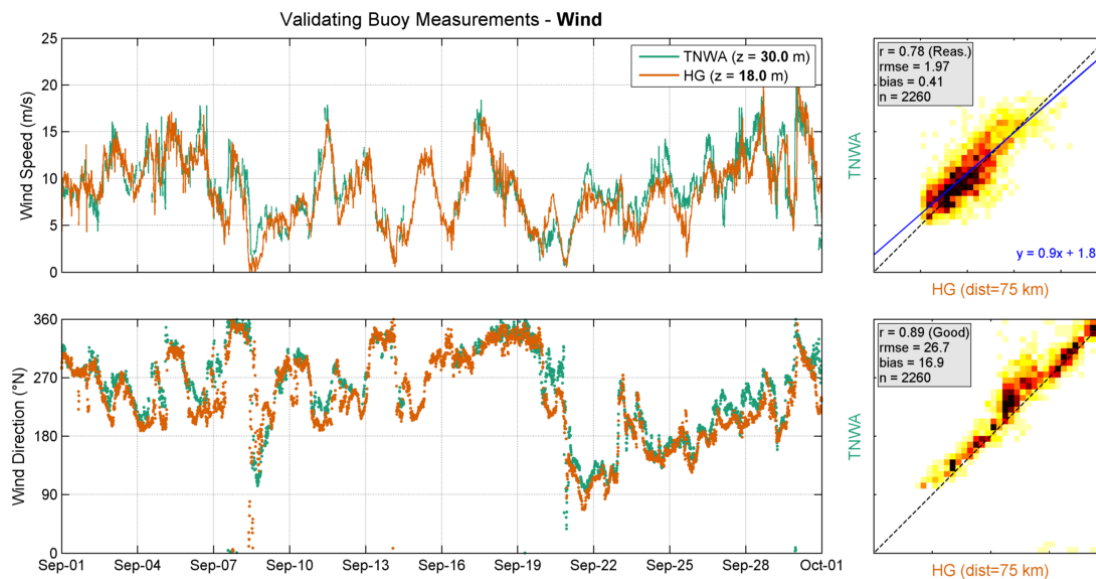
Figure 3.12: *Validation of TNWA (data from September 2019) with HG wind data. Left panel: Timeseries. Middle panel: Density scatter, with the darker colours indicating more data density.*

3.2.2.2   LiDAR

In the following the TNWA wind data are compared with the LiDAR observations at K13. Before comparing the TNWA data with the K13 LiDAR data, these are validated against the anemometer data at K13. Figure 3.13 shows the comparison between the K13 LiDAR and anemometer timeseries. A timeseries comparison is provided showing the LiDAR data at levels 63 m, 91 m, 116 m, 141 m, 166 m and 191 m and the single level (73.8 m) anemometer data, with a density scatter comparing the LiDAR measurements at the 63 m level with the fixed anemometer observations at the 73.8 m level (best match in terms of elevation). The correlations are excellent in terms of both wind speed and direction. As expected due to the difference in elevation (73.8 and 63 m), there is a bias in the wind speed, with the (observed at a higher height) anemometer wind speeds being on average slightly higher.

Table 3.2 shows the comparisons between the TNWA observations and those of the closer vertical levels by the LiDAR at K13. As was also the case in the comparisons with the K13 anemometer, the comparisons are at all levels poor in terms of wind speed and reasonable in terms of direction. The low correlations are based on our experience due to the low wind speeds characterizing the period, which also explain the increase in correlations with height given that the wind speeds also on average increase with height.
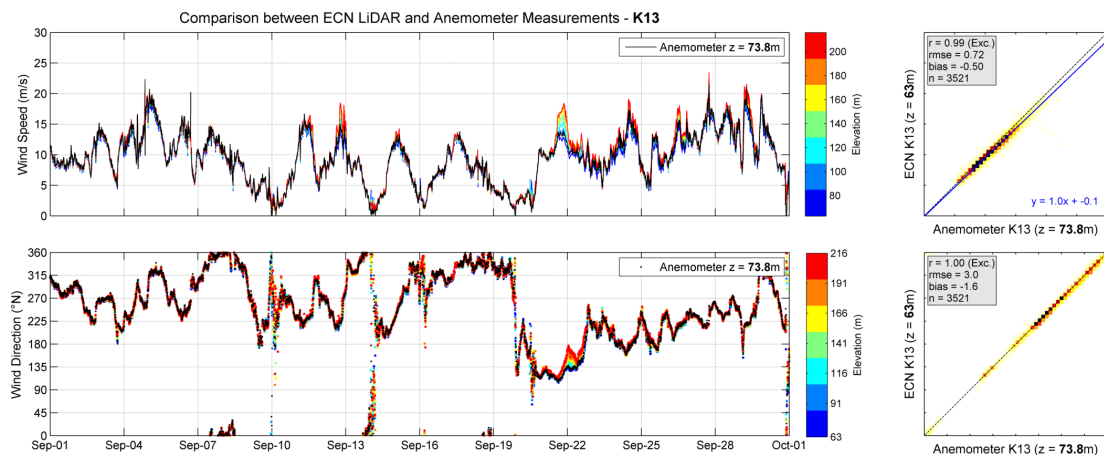
Figure 3.13: *Comparison between ECN LiDAR and anemometer measurements at K13.*

Table 3.2: *Statistical comparison between TNWA and K13 LiDARs at different heights.*

Elevation		Wind Speed				Wind Direction		
TNWA (m)	K13 (m)	r (-)	Bias (m/s)	Symmetrical Slope (-)	n (-)	r (-)	Bias ($^\circ$N)	n (-)
60	63	0.55	-0.20	0.98	2297	0.77	5.8	2297
100	91	0.55	-0.22	0.98	2321	0.78	5.9	2321
120	116	0.56	-0.14	0.98	2332	0.78	5.6	2332
140	141	0.57	-0.08	0.99	2349	0.78	5.4	2349
160	166	0.58	-0.06	0.99	2352	0.78	5.5	2352
200	191	0.60	-0.14	0.99	2363	0.78	5.2	2363
250	241	0.61	-0.21	0.98	2376	0.78	5.5	2376

3.2.3 Ten Noorden van de Waddeneilanden Buoy TNWB

3.2.3.1 Anemometer

As shown for TNWA, Figure 3.14, Figure 3.15, Figure 3.16, Figure 3.17, Figure 3.18 and Figure 3.19 show comparisons between TNWB observations and those at L91, F161, K13, F3, AWG, and HG, respectively. The correlation, root-mean-square error and bias statistics are printed in the figures.

As can be seen in the figures, the comparisons between the TNWB observations (which only cover the period until the 12th of September) and those from:

- L91, F161, F3 and AWG are reasonable in terms of wind speed and good in terms of wind direction,
- K13 are poor in terms of wind speed and reasonable in terms of wind direction, and
- HG are reasonable in terms of both wind speed and direction.
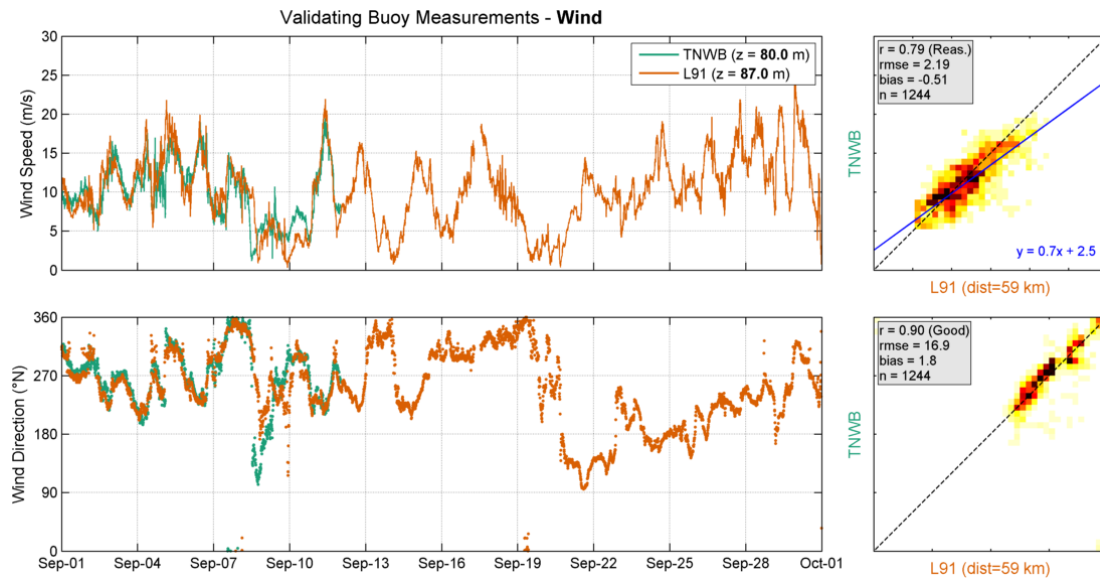
Figure 3.14: *Validation of TNWB (data from September 2019) with L19 wind data. Left panel: Timeseries. Middle panel: Density scatter, with the darker colours indicating more data density.*
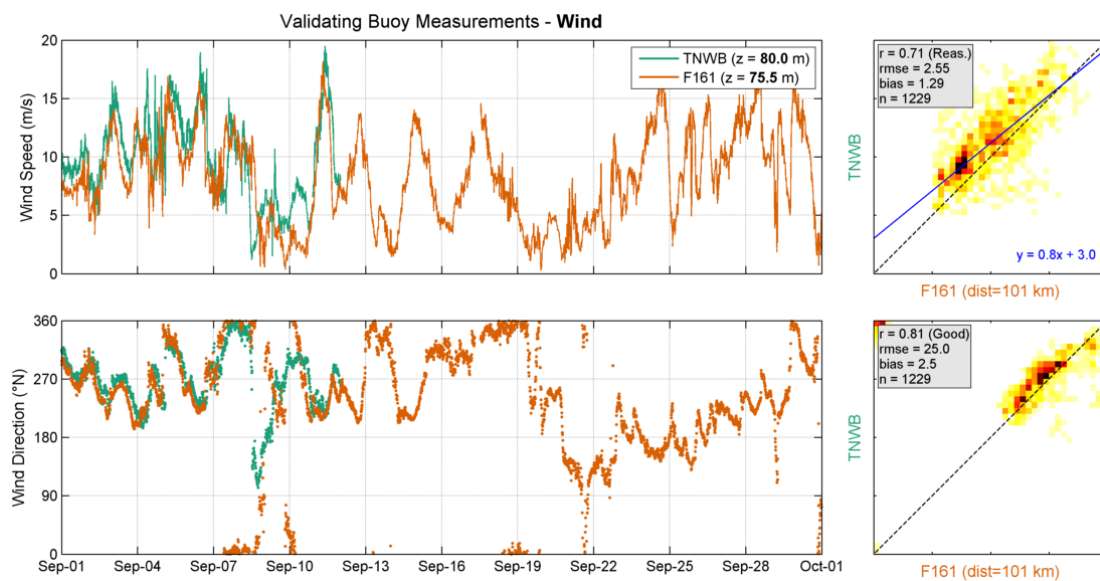
Figure 3.15: *Validation of TNWB (data from September 2019) with F161 wind data. Left panel: Timeseries. Middle panel: Density scatter, with the darker colours indicating more data density.*
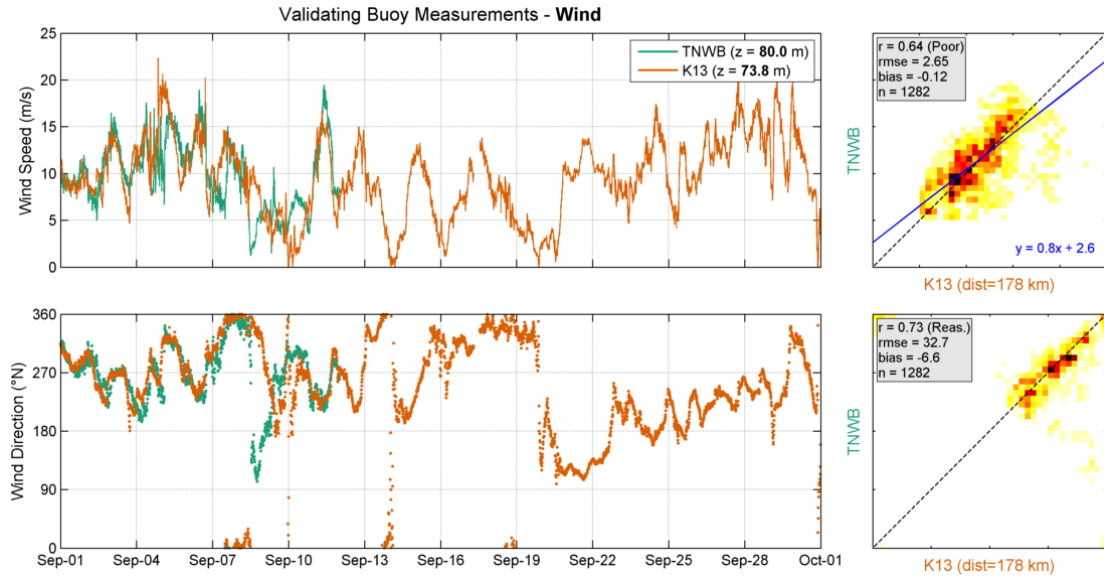
Figure 3.16: *Validation of TNWB (data from September 2019) with K13 wind data. Left panel: Timeseries. Middle panel: Density scatter, with the darker colours indicating more data density.*
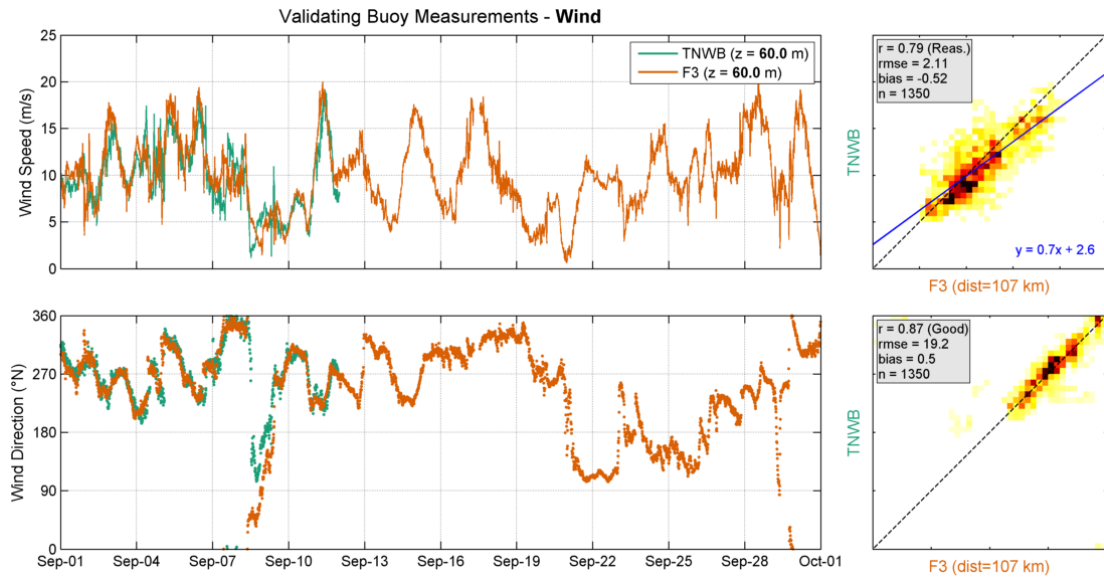
Figure 3.17: *Validation of TNWB (data from September 2019) with F3 wind data. Left panel: Timeseries. Middle panel: Density scatter, with the darker colours indicating more data density.*
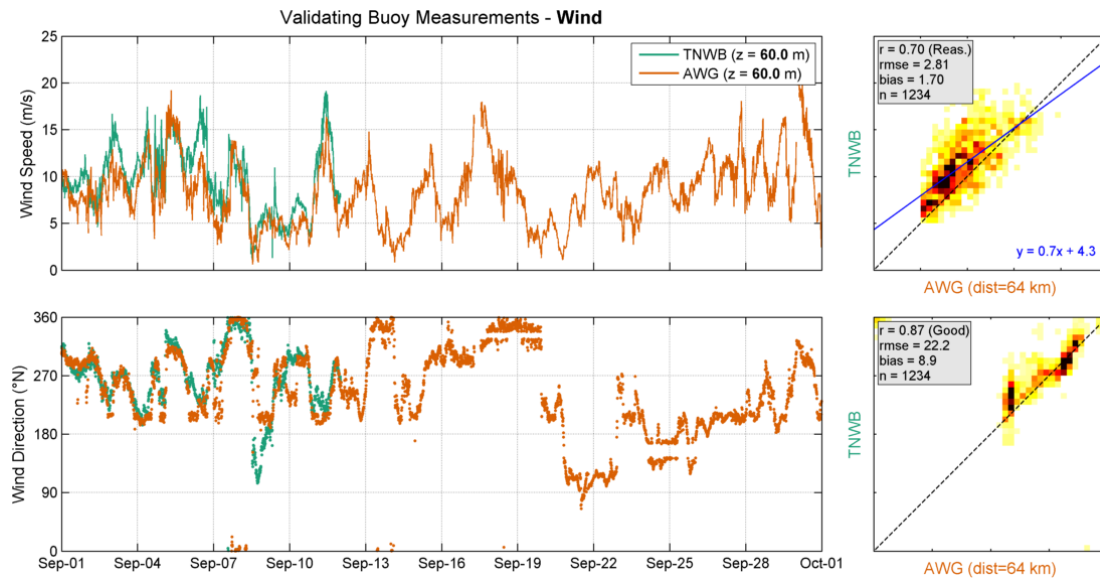
Figure 3.18: *Validation of TNWB (data from September 2019) with AWG wind data. Left panel: Timeseries. Middle panel: Density scatter, with the darker colours indicating more data density.*
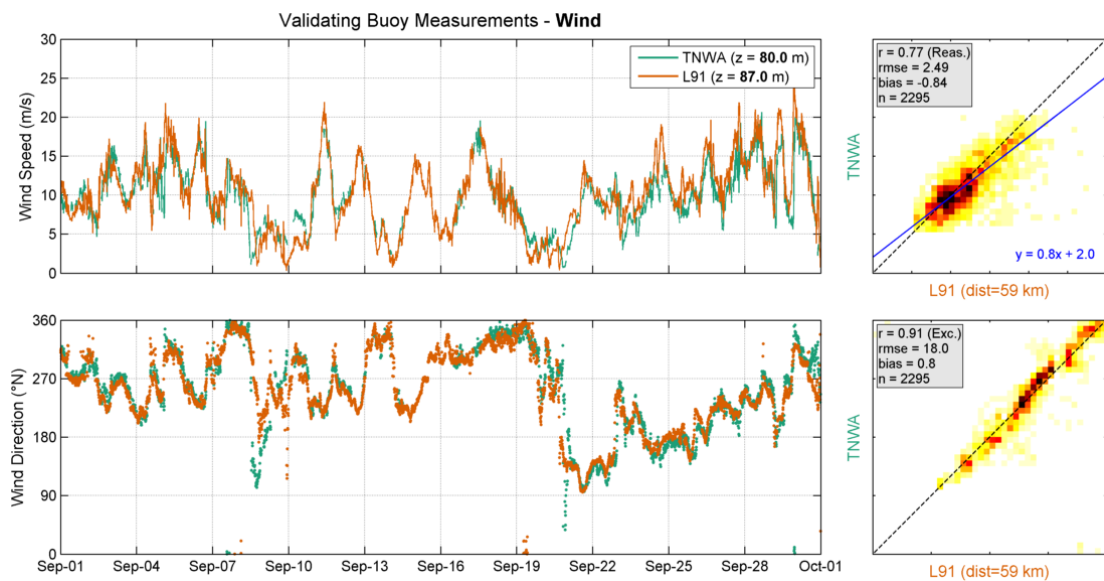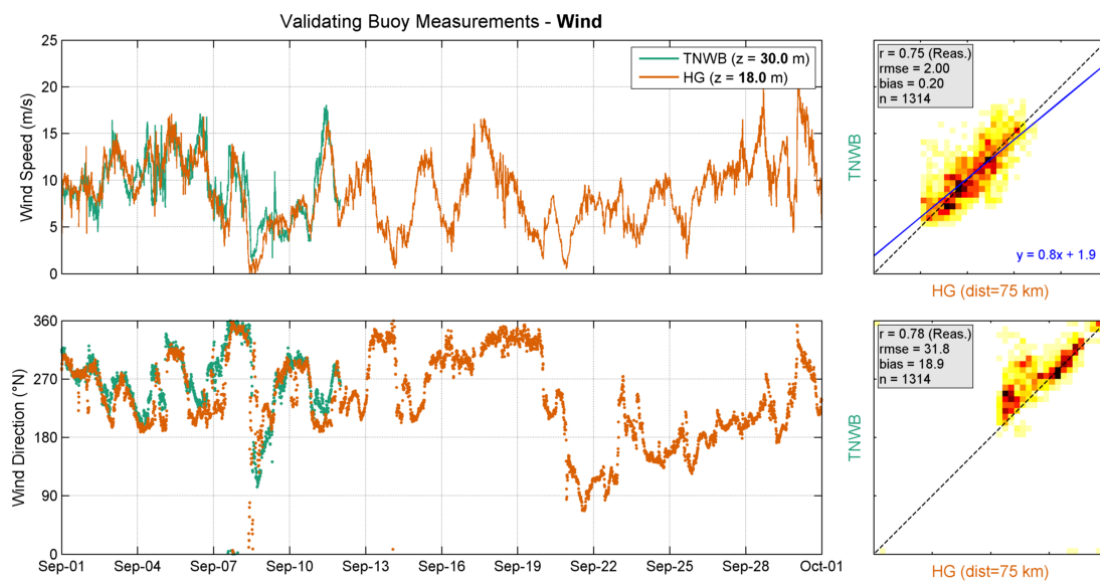

Figure 3.19: *Validation of TNWB (data from September 2019) with HG wind data. Left panel: Timeseries. Middle panel: Density scatter, with the darker colours indicating more data density.*

3.2.3.2 LiDAR

Table 3.3 show the error statistics between the TNWB observations and those of the closer vertical levels by the LiDARs at K13. As was also the case in the comparisons between the TNWA and K13 data and between the TNWB and K13 anemometer data, the comparisons are poor in terms of wind speed and reasonable in terms of wind direction.

Table 3.3: *Statistical comparison between TNWB and K13 LiDARs at different heights.*

Elevation		Wind Speed				Wind Direction		
TNWB (m)	K13 (m)	r (-)	Bias (m/s)	Symmetrical Slope (-)	n (-)	r (-)	Bias (°N)	n (-)
60	63	0.63	-0.25	0.98	1265	0.75	4.3	1265
100	91	0.64	-0.28	0.97	1280	0.73	4.8	1280
120	116	0.65	-0.25	0.98	1290	0.72	4.6	1290
140	141	0.66	-0.24	0.98	1293	0.73	4.2	1293
160	166	0.66	-0.23	0.98	1299	0.73	4.2	1299
200	191	0.67	-0.29	0.97	1307	0.72	4.0	1307
250	241	0.68	-0.35	0.97	1312	0.72	4.6	1312

3.2.4 Spatial and temporal variability

In order to further evaluate the spatial variations in the observation period, the wind fields from the Dutch Meteorological Institute (KNMI) operational Numerical Weather Prediction model Hirlam7.2 are also considered. The model fields are only available at 10 m and with an hourly resolution. The spatial resolution of the model is about 11 km x 11 km, which implies that the model in principle underestimates the spatial variations and coastal effects, i.e. the model results can be expected to be smoother than the true fields.

In order to characterize further the most extreme events in the observation period, Figure 3.20 and Figure 3.21 show the model wind fields at the hour of the maximum observed 100 m wind speed TNWA and TNWB, respectively.

The maximum observed 100 m wind speed at TNWA is on the 30th at around 01:00 (cf. Figure 3.2), in a period of surface winds from the Northwest, with the highest wind speeds occurring close to the shore, see Figure 3.20.

The maximum observed 100 m wind speed at TNWB is on the 11th at around 10:00, in a period of surface winds from the Southeast, with a diagonal band of higher winds speeds stretching from L91 to the TNW region and further to the Northeast.
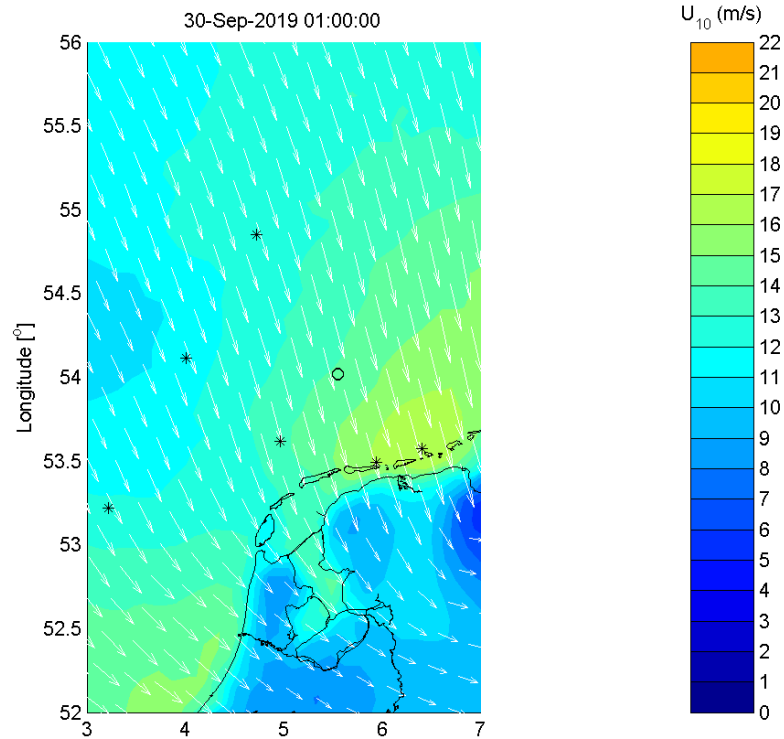
Figure 3.20: *Hirlam7.2 surface wind field at the hour of the maximum TNWA 100 m wind speed. The *s indicate the locations of the fixed stations and the ∘s the TNW locations.*
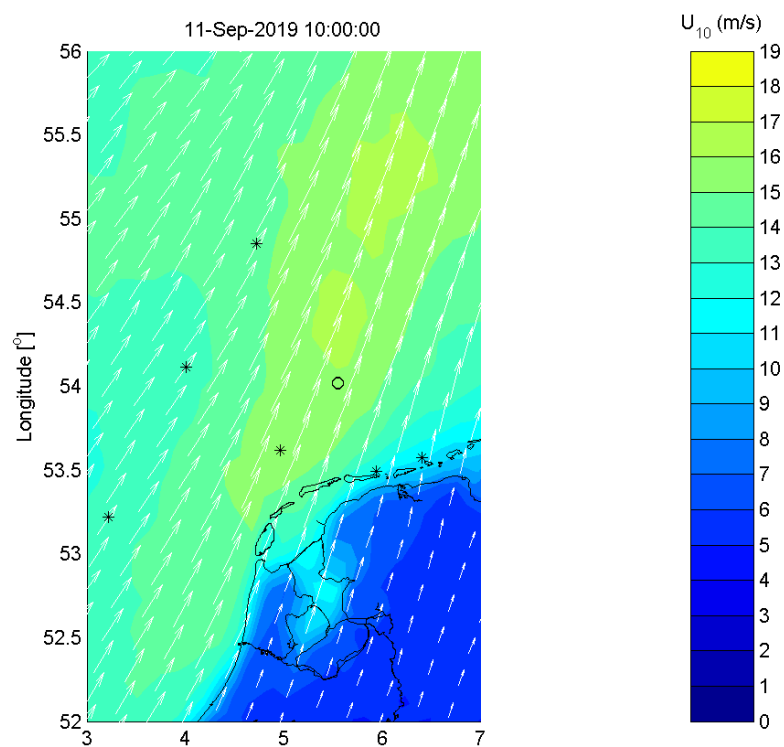
Figure 3.21: *Hirlam7.2 surface wind field at the hour of the maximum TNWB 100 m wind speed. The *s indicate the locations of the fixed stations and the ∘s the TNW locations.*

Table 3.4 shows the correlations between the Hirlam7.2 10 m (hourly) wind speeds and directions from the model grid points closer to the buoy and the fixed station locations at the timestamps at which the data from each of the buoys are valid. Given the proximity of the TNWA and TNWB locations the considered model grid point is the same, therefore differences between correlations with the data at the TNWA and TNWB locations are only due to differences in measurement data availability. For these periods the corresponding correlations between the buoy and the fixed station anemometer (10 minute) observations (at the closer vertical levels) are given in figures 3.7 to 3.12 and 3.14 to 3.19 and reproduced Table 3.5. As can be seen in Table 3.4, the model winds at TNW have the higher correlations with the winds at the L91 and AWG locations and the lowest with the winds at K13. The comparison of the correlations between the observations and the models results confirm that the found discrepancies are mostly due to spatial variations (note also the low correlations between the TNW and K13) and local effects (such as land effects at AWG and HG) which are less present in the model results due to its resolution.

Table 3.4: *Statistical comparison between the model results at the buoy and at the fixed station locations at the timestamps at which the buoy data are valid*

	TNWA			**TNWB**		
Station	U_{10} r **(-)**	U_{dir} r **(-)**	n **(-)**	U_{10} r **(-)**	U_{dir} r **(-)**	n **(-)**
L91	0.89	0.95	422	0.91	0.94	239
F161	0.77	0.88	422	0.83	0.78	239
K13	0.58	0.73	422	0.74	0.62	239
F3	0.84	0.89	422	0.90	0.91	239
AWG	0.92	0.96	422	0.92	0.93	239
HG	0.85	0.91	422	0.87	0.84	239

Table 3.5: *Statistical comparison between the TNWA and TNWB buoy observations and those from the fixed stations.*

	TNWA				**TNWB**			
Station	U_{10} r **(-)**	n **(-)**	U_{dir} r **(-)**	n **(-)**	U_{10} r **(-)**	n **(-)**	U_{dir} r **(-)**	n **(-)**
L91	0.77	2295	0.91	2295	0.79	1244	0.90	1244
F161	0.61	2057	0.86	2057	0.71	1229	0.81	1229
K13	0.56	2289	0.77	2289	0.64	1282	0.73	1282
F3	0.79	2375	0.86	2375	0.79	1350	0.87	1350
AWG	0.71	2287	0.90	2287	0.70	1234	0.87	1234
HG	0.78	2260	0.89	2260	0.75	1314	0.78	1314

In order to assess to which extent the difference in the correlations between the TNWA and TNWB wind and those from the fixed stations are due to the differences in the periods covered by the data, Table 3.6 shows the correlations between the TNWA and TNWB buoy observations and those from the fixed stations at the timestamps at which the data from both buoys are valid (until the 12th of September 2019). As can be seen in Table 3.6, when restricting the comparisons to the overlapping dates, then the correlations are almost identical, as could already be expected from the high correlations between the collocated buoy data (cf. Table 3.1).

Table 3.6: *Statistical comparison between the TNWA and TNWB buoy observations and those from the fixed stations at the timestamps at which the data from both buoys are valid.*

Station	TNWA				TNWB			
	U_{10} r (-)	n (-)	U_{dir} r (-)	n (-)	U_{10} r (-)	n (-)	U_{dir} r (-)	n (-)
L91	0.78	800	0.90	800	0.78	800	0.90	800
F161	0.70	797	0.80	797	0.70	797	0.80	797
K13	0.66	843	0.72	843	0.65	843	0.72	843
F3	0.79	879	0.86	879	0.79	879	0.85	879
AWG	0.69	801	0.89	801	0.69	801	0.89	801
HG	0.78	855	0.81	855	0.78	855	0.81	855

3.3 Conclusions

Based on the comparisons between the data from the buoys, which are excellent at all levels and within the best practice range (and in accordance with KPIs obtained during the pre-validation of the LiDARs), the validation of the data against observations and model data, which shows mismatches can be explained by local effects and spatial variations, it can be concluded that the accuracy of the TNW buoy wind speeds and directions is high.

4 Waves

The measured waves from both buoys are presented and analyzed within this chapter. The goal is to assess the reliability and accuracy of the retrieved wave data from both TNWA and TNWB. This is completed by first comparing the integral parameters from both buoys against each other, followed by a statistical validation against fixed wave measurements in the area.

4.1 Overview

The timeseries of the main wave parameters for both TNWA and TNWB is shown in Figure 4.1. It includes the following parameters:

- significant wave height, H_s
- peak wave period, T_p
- mean wave direction, MWD
- swell and sea[1] significant wave heights, H_{sswell} and H_{ssea}
- maximum wave height, H_{max}
- swell and sea mean wave directions, MWD_{swell} and MWD_{sea}
- mean wave periods, T_{m01} and T_{m02}, and
- swell and sea mean wave periods, $T_{m02swell}$ and T_{m02sea}.

The most predominant and higher waves are from the Northwest, which are as expected associated with the longer wave periods. The two buoys at Ten Noorden van de Waddeneilanden agree extremely well given the near-identical signals (e.g. H_s, T_{m02}, etc ...) with only short term discrepancies between the peak wave period and the mean wave direction of swell. These are expected given that these parameters depend more strongly on the sampling variability (randomness of the sea surface elevation) and discreteness of the wave spectra.

---

[1]The swell and sea variables are computed from the spectral energy in the frequency band between respectively 0.04 and 0.10 Hz and 0.10 and 0.50 Hz (cf. Table 2.1).
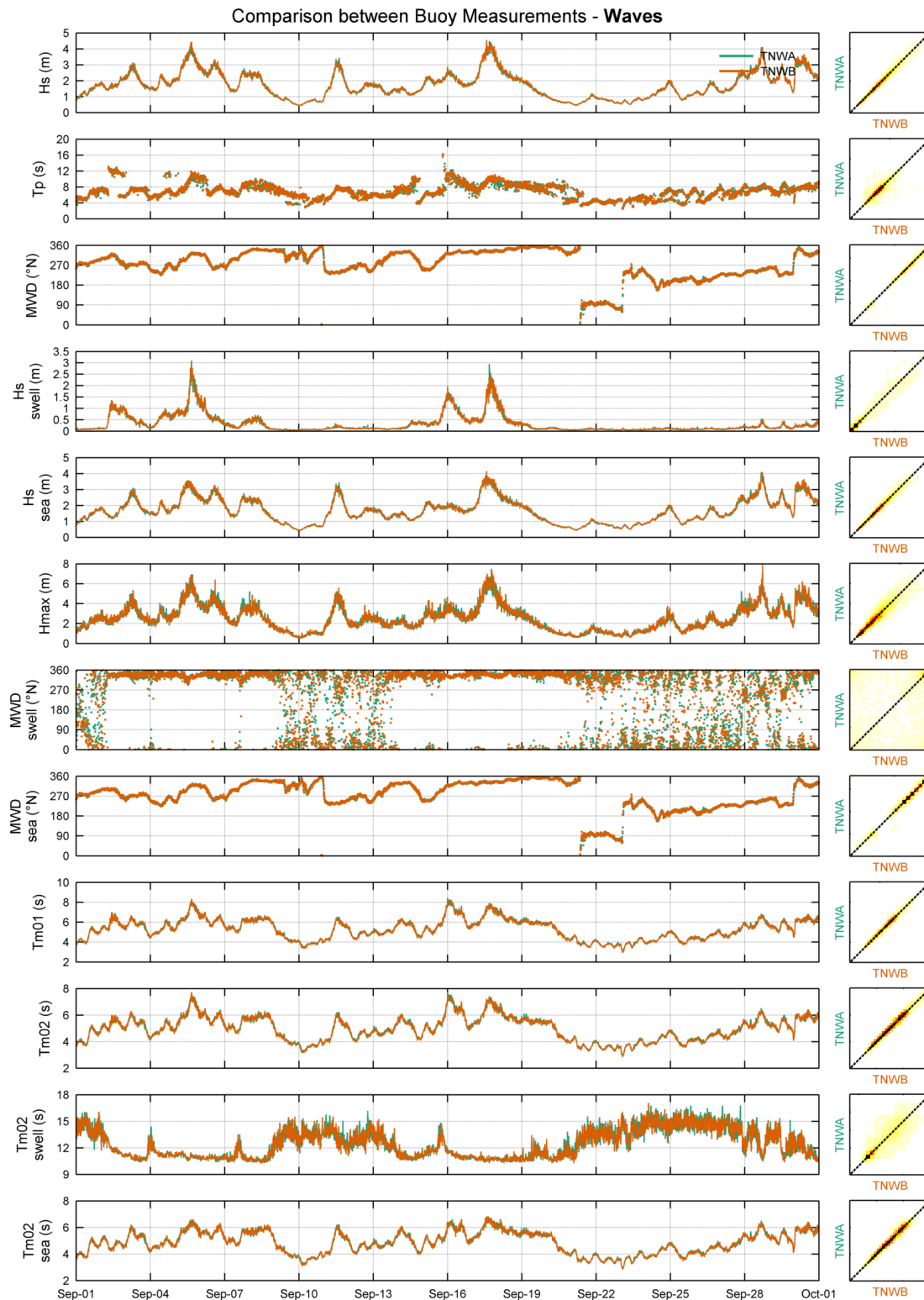
Figure 4.1: *Wave parameters at each buoy (data from September 2019).*

The slope, bias, correlations and square correlations were calculated for all wave parameters measured at TNWA and TNWB to quantify their statistical differences, see Table 4.1. As can be seen in the table, the agreement between the two buoys is excellent in terms of all parameters, except in terms of peak wave period which is good and mean wave direction of swell which is poor. The mismatches in the mean wave direction of swell are in periods with

almost no swell energy (cf. Figure 4.1). These low levels of energy explain the variability in the resulting swell direction but also make it less important.

Table 4.1: Statistical comparison between TNWA and TNWB wave parameters.

Parameter	Unit	r^2 (-)	r (-)	Bias (unit)	Symmetrical Slope (-)	n (-)
hm0	m	0.98	0.99	0.01	1.01	4309
tp	s	0.75	0.87	-0.01	1.00	4309
mdir	°N	0.98	0.99	0.28	1.00	4309
hm0a	m	0.97	0.98	0.00	1.01	4309
hm0b	m	0.98	0.99	0.01	1.01	4309
hmax	m	0.89	0.94	0.02	1.01	4309
mdira	°N	0.06	0.24	0.32	1.00	4309
mdirb	°N	0.99	0.99	0.26	1.00	4309
tm01	s	0.98	0.99	-0.02	1.00	4309
tm02	s	0.98	0.99	-0.02	1.00	4309
tm02a	s	0.82	0.91	-0.01	1.00	4309
tm02b	s	0.97	0.99	-0.02	1.00	4309

4.2 Validation

An overview of the comparisons is first presented, followed by a detailed comparison between the data from TNWA (Section 4.2.2) and TNWB (Section 4.2.3) with the fixed observations.

4.2.1 Overview

Figure 4.2 and Figure 4.3 show the significant wave height and peak wave period roses, respectively, at TNWA, TNWB and SON. No roses are shown for F161 and F3 because there are no wave direction observations available from these platforms. The roses show an overall agreement, especially when considering their locations. At all locations the severer and most predominant waves are from the Northwest and, given its location nearer the shore (cf. Figure 1.2), there are less waves from Southwest and the Eastern waves have due to refraction a more northern alignment at SON.
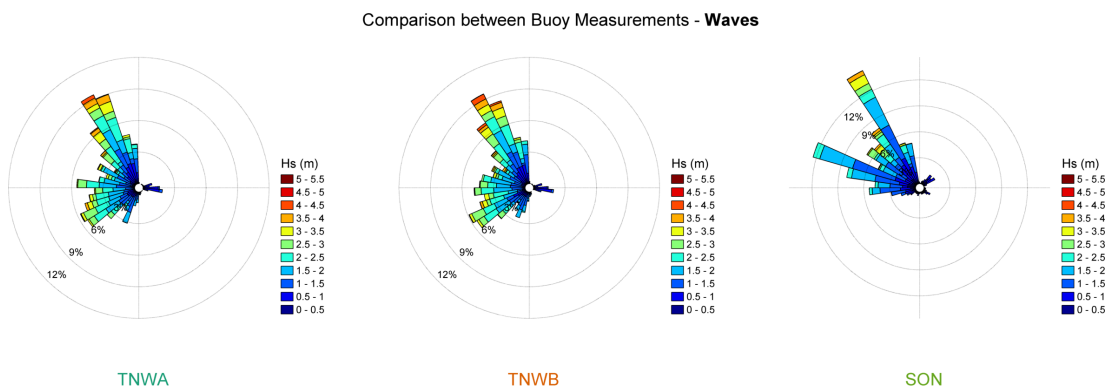
Figure 4.2: Significant wave height roses (data from September 2019).

Comparison between Buoy Measurements - **Waves**
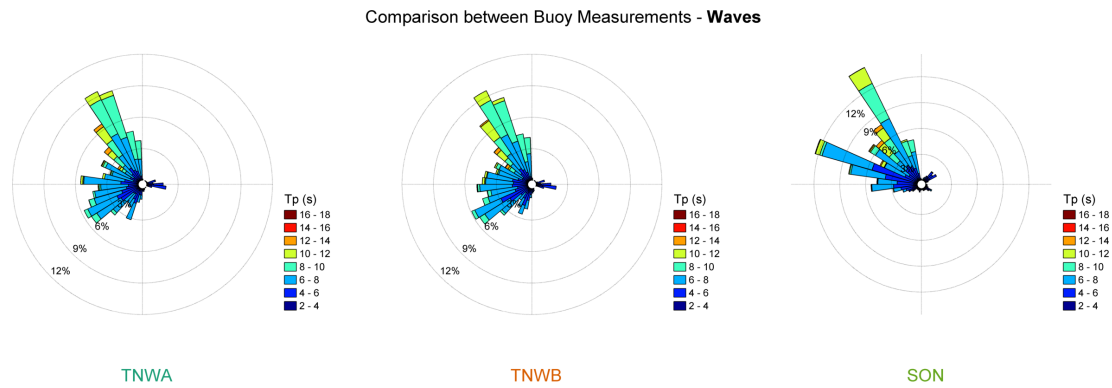
Figure 4.3: *Peak wave period roses (data from September 2019).*

4.2.2 Ten Noorden van de Waddeneilanden Buoy TNWA

Figure 4.4, Figure 4.5 and Figure 4.6 show comparisons between TNWA observations and those at F161, F3 and SON of H_s, T_p, mean wave period, $T_{m0,2}$, and mean wave direction, MWD (only SON, Figure 4.6). The correlation, root-mean-square error and bias statistics are printed in each of the figures.

As can be seen in the figures, the comparisons between TNWA observations and those:

- at F161 are excellent in terms of significant and swell wave height, good in terms of mean wave period and reasonable in terms of peak wave period;
- at F3 are excellent in terms of significant wave height, swell wave height and mean wave period and reasonable in terms of peak wave period; and
- at SON are excellent in terms of swell wave height, good in terms of significant wave height and mean wave period and reasonable in terms of peak wave period and mean wave direction.

Discrepancies between the mean wave direction at TNW and SON are expected given the shallower and closer to the shore location of SON (cf. Figure 1.2). Discrepancies in terms of peak wave period between the data from all locations are also expected given the discrete characteristics of the variable.
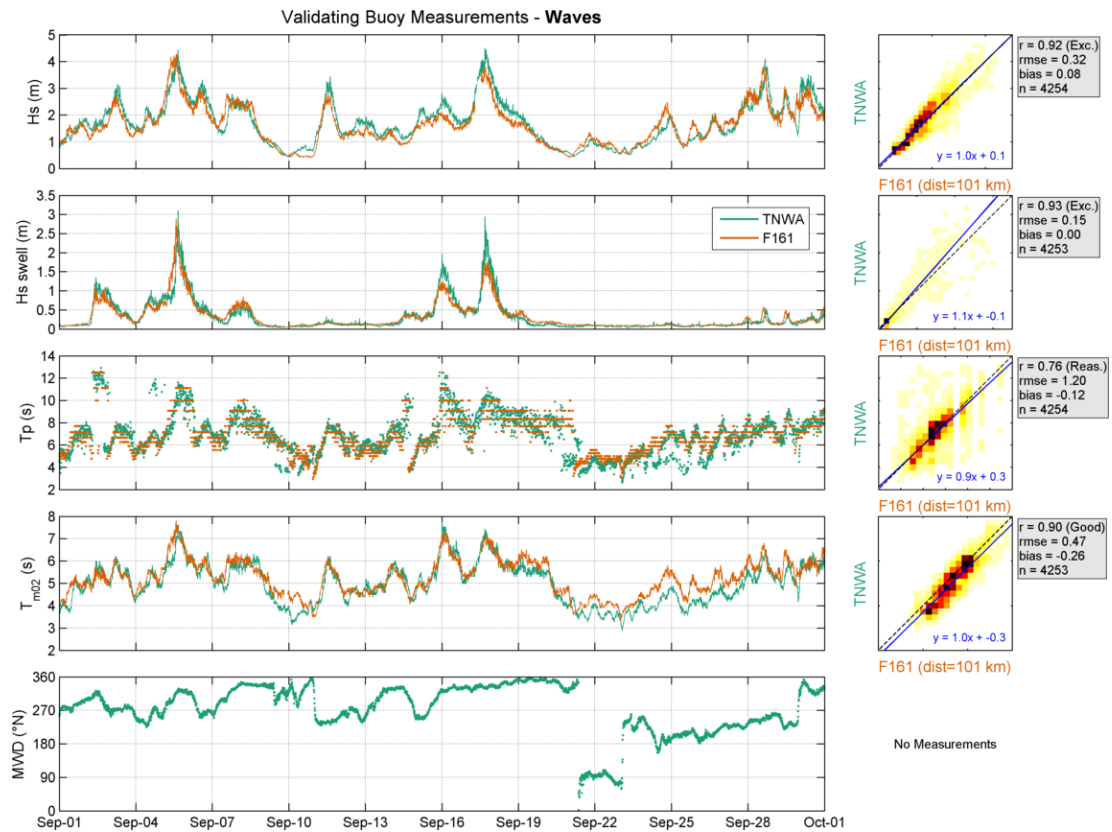
Figure 4.4: *Validation of TNWA (data from September 2019) with F161 wave data. Left panel: Timeseries. Middle panel: Density scatter, with the darker colours indicating more data density.*
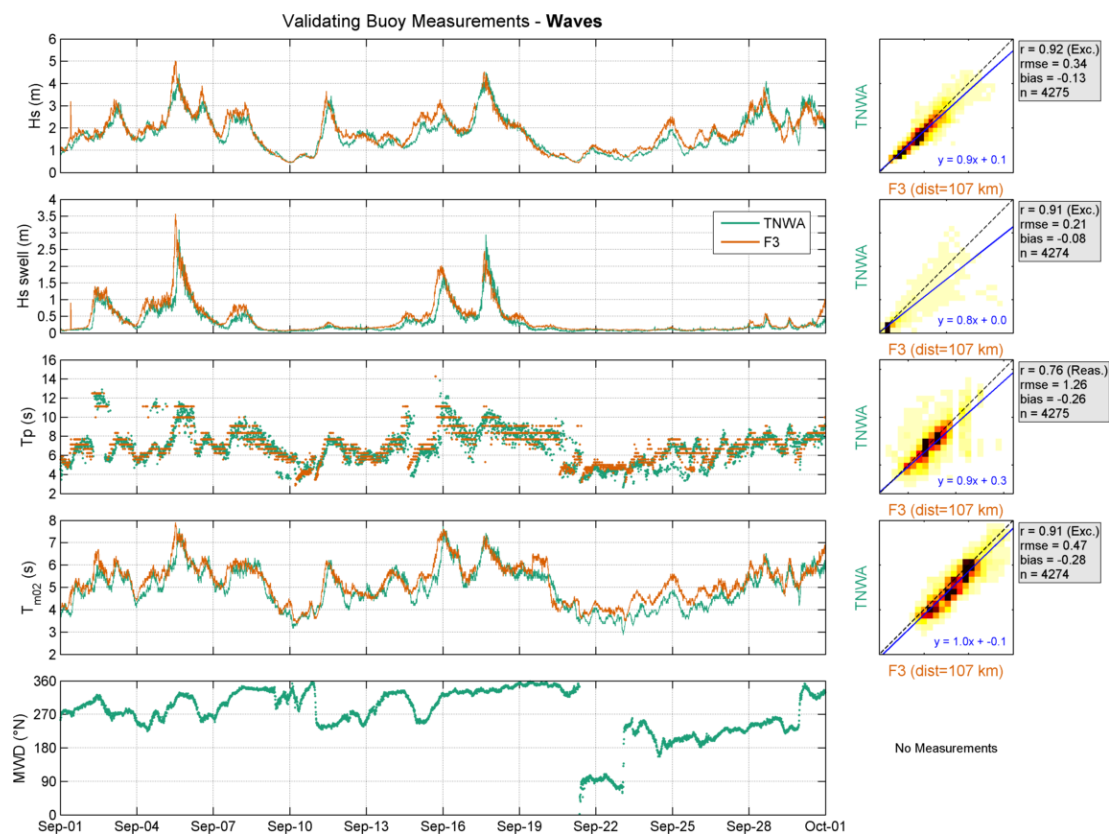
Figure 4.5: *Validation of TNWA (data from September 2019) with F3 wave data. Left panel: Timeseries. Middle panel: Density scatter, with the darker colours indicating more data density.*
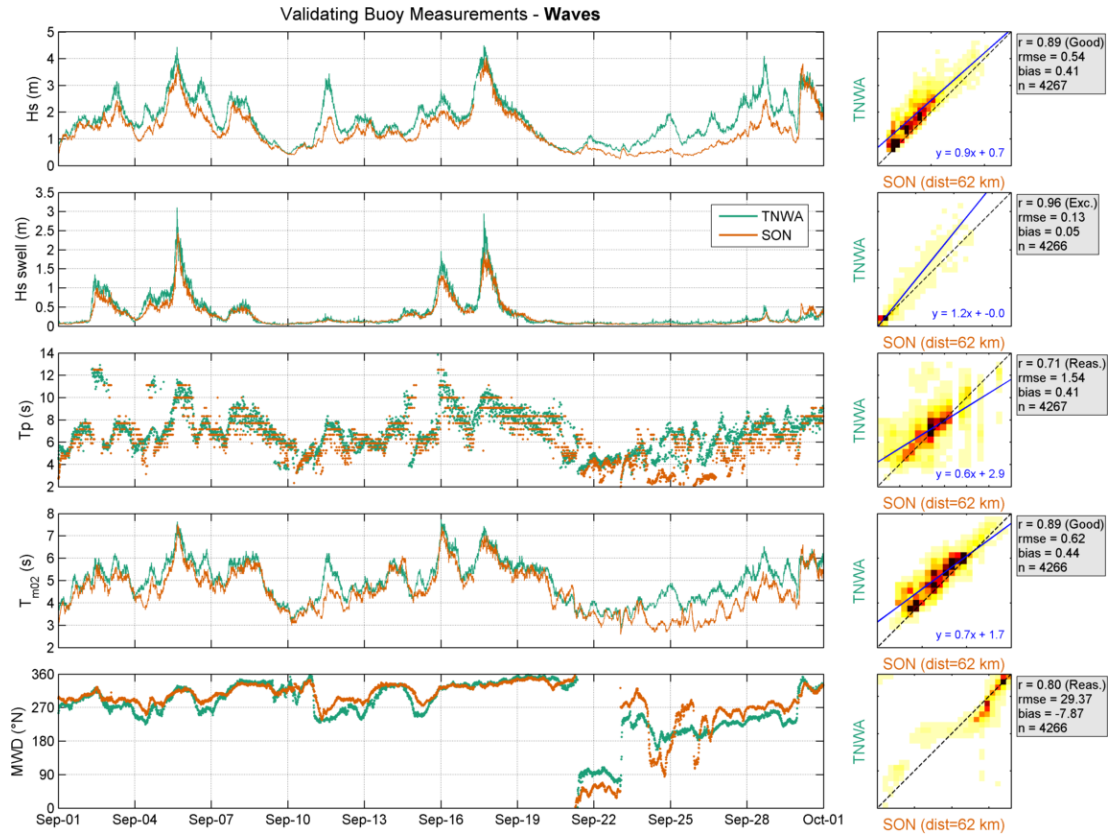
Figure 4.6: *Validation of TNWA (data from September 2019) with SON wave data. Left panel: Timeseries. Middle panel: Density scatter, with the darker colours indicating more data density.*

4.2.3 Ten Noorden van de Waddeneilanden Buoy TNWB

Figure 4.7, Figure 4.8 and Figure 4.9 show comparisons between TNWB observations and those at F161, F3 and SON of H_s, T_p, mean wave period, $T_{m0,2}$, and mean wave direction, MWD (only SON, Figure 4.9). The correlation, root-mean-square error and bias statistics are printed in each of the figures. The comparisons between the TNWB and the fixed station data are in line with those between the TNWA and the fixed station data.
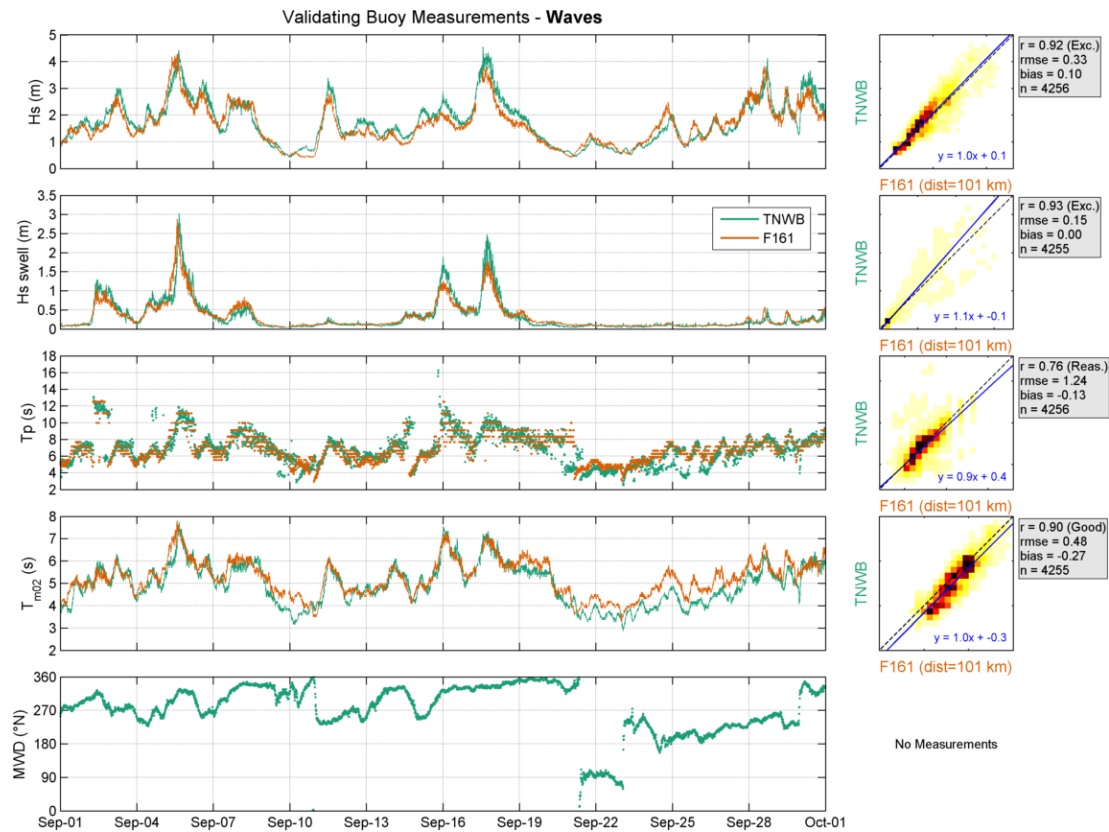
Figure 4.7: *Validation of TNWB (data from September 2019) with F161 wave data. Left panel: Timeseries. Middle panel: Density scatter, with the darker colours indicating more data density.*
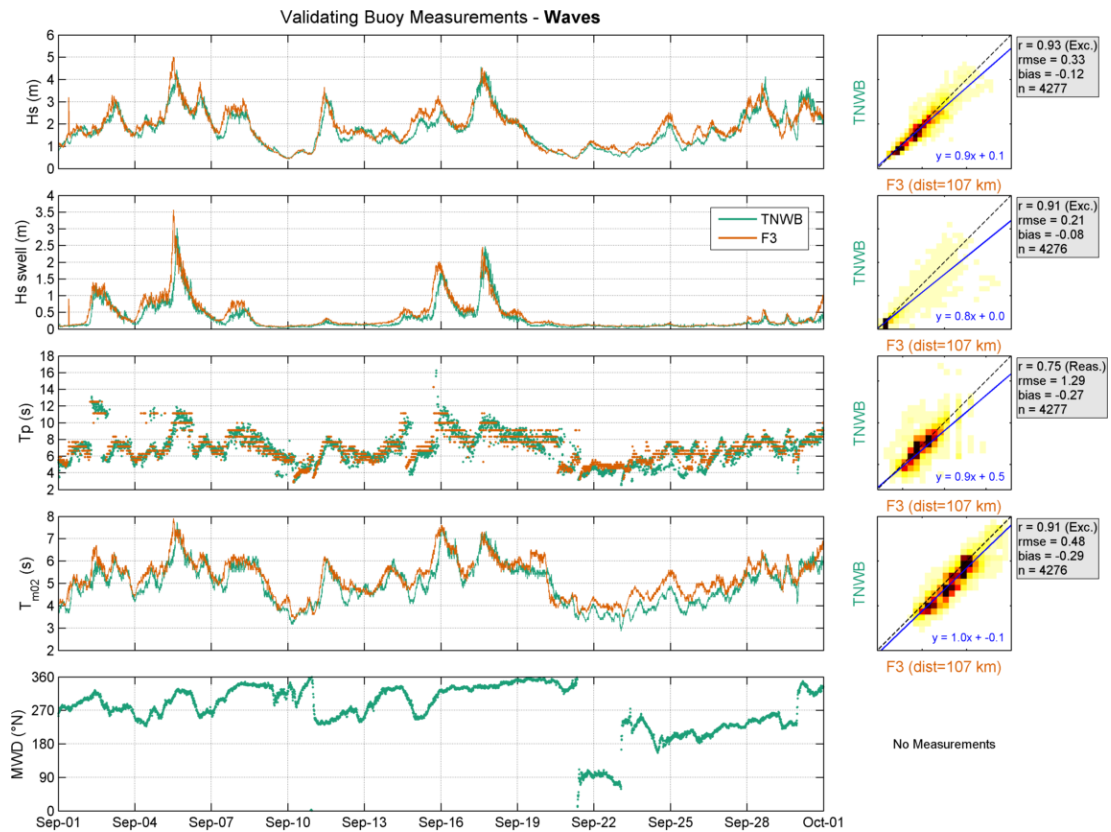
Figure 4.8: *Validation of TNWB (data from September 2019) with F3 wave data. Left panel: Timeseries. Middle panel: Density scatter, with the darker colours indicating more data density.*
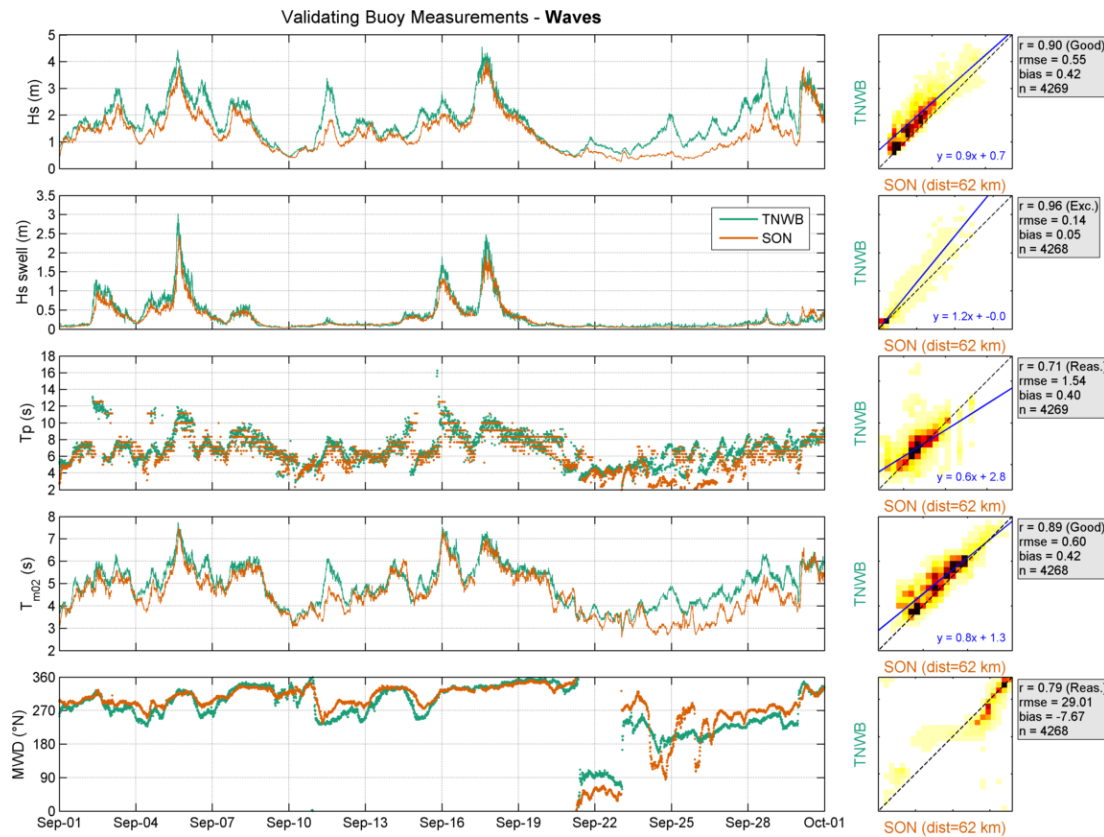
Figure 4.9: *Validation of TNWB (data from September 2019) with SON wave data. Left panel: Timeseries. Middle panel: Density scatter, with the darker colours indicating more data density.*

4.3 Summary and conclusions

The correlations between the buoy and the fixed station wave observations given in figures 4.4 to 4.6 and 4.7 to 4.9 are summarized in Table 4.2.

Table 4.2: *Statistical comparison between the TNWA and TNWB buoy observations and those from the fixed stations.*

	TNWA			TNWB		
Station	F161	F3	SON	F161	F3	SON
$H_s\ r$ **(-)**	0.92	0.92	0.89	0.92	0.93	0.90
$H_s\ n$ **(-)**	4254	4275	4267	4256	4277	4269
$H_{sswell}\ r$ **(-)**	0.93	0.91	0.96	0.93	0.91	0.96
$H_{sswell}\ n$ **(-)**	4253	4274	4266	4255	4276	4268
$T_p\ r$ **(-)**	0.76	0.76	0.71	0.76	0.75	0.71
$T_p\ n$ **(-)**	4254	4275	4267	4256	4277	4269
$T_{m02}\ r$ **(-)**	0.90	0.91	0.89	0.90	0.91	0.89
$T_{m02}\ n$ **(-)**	4253	4274	4266	4255	4276	4268
$MWD\ r$ **(-)**	-	-	0.80	-	-	0.79
$MWD\ n$ **(-)**	-	-	4266	-	-	4268

Based on a) the comparisons between the data from the buoys, which are excellent for all parameters, except as expected those depending strongly on the sampling variability (randomness of the sea surface elevation) and discreteness of the wave spectra (T_p and MWD_{swell}, cf. Table 4.1), and b) the validation of the data against the platform

observations, in which mismatches can be explained by local effects, spatial variations and again discreteness of the wave spectra, it can be concluded that the accuracy of the TNW buoy wave data is high.

5 Temperature

During this deployment period air and surface water temperatures are measured at both buoys and the bottom water temperature by the WLS at TNWB (cf. Figure 2.1).

5.1 Overview

Figure 5.1 shows the observed air and water temperature and their differences. As expected, given their distance from the surface, the WLS observations are those that vary more smoothly in time. They are furthermore, close to the surface temperature observations. However, given that the temperature sensor in the WLS has not been calibrated, it can be that the bottom temperature observations are biased. They are, nevertheless, shown for illustration of their temporal variations, which are in principle measured accurately.
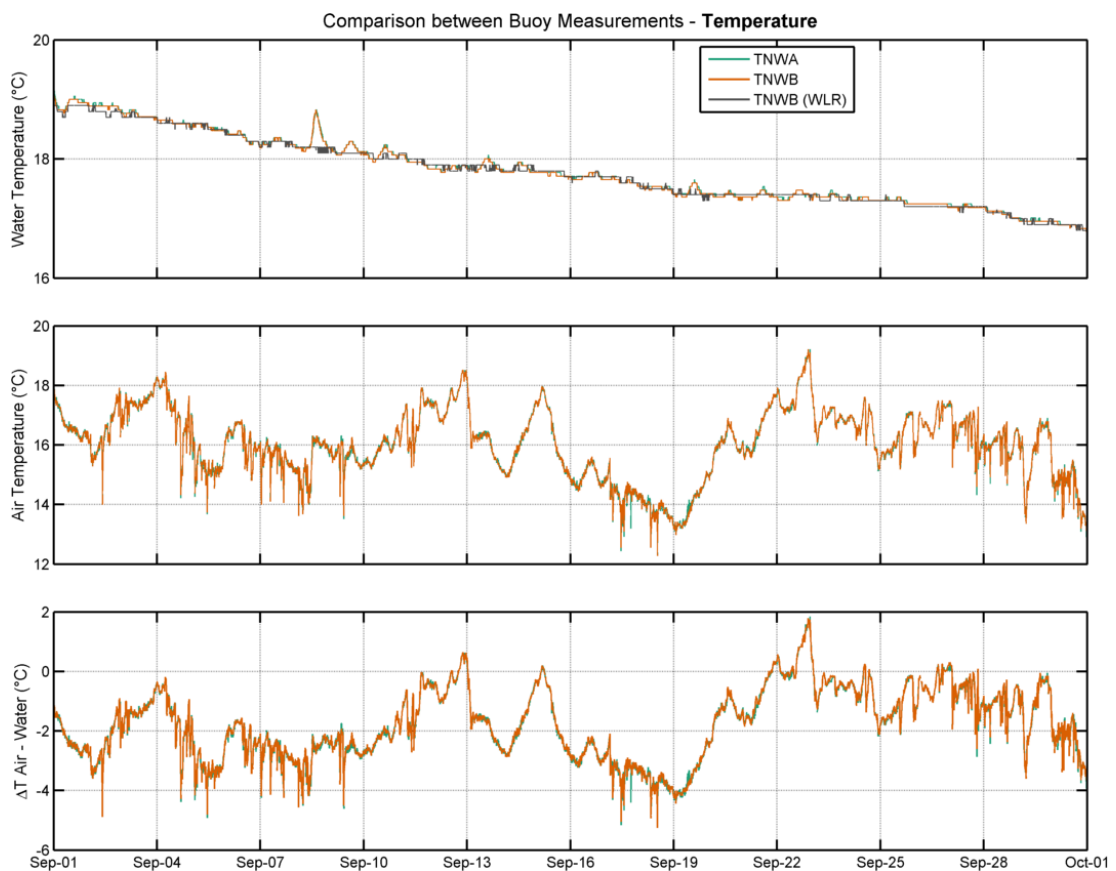
Figure 5.1: *Temperature difference measured at LiDAR buoys (data from September 2019).*

5.2 Validation

The comparisons between fixed station measurements and the TNW data are presented in Section 5.2.1 (water temperature) and in Section 5.2.2 (air temperature).

5.2.1 Water Temperature

A timeseries comparison between the observations from both buoys and sensors and the fixed stations is presented in Figure 5.2. The water temperature observations from the fixed

stations are all surface temperatures. Figure 5.2 shows that during September the warmest and coolest temperatures and larger (lower) temporal gradients and daily variations are observed at SON (K13).
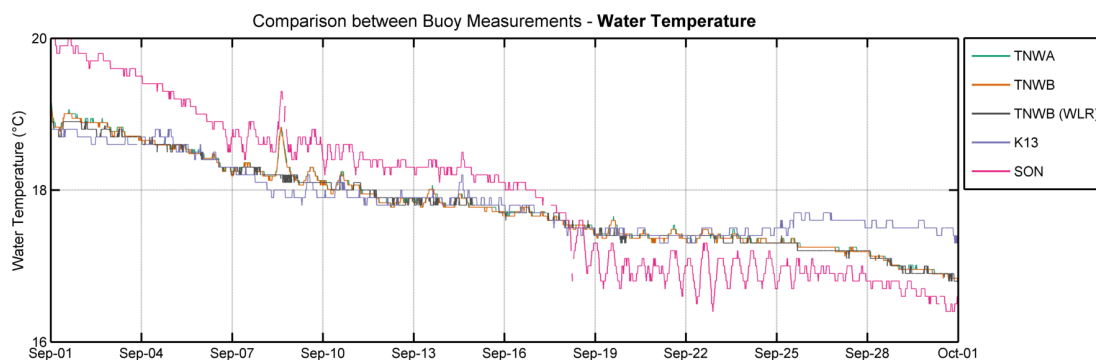
Figure 5.2: *Water temperature measurements from all locations (data from September 2019).*

A direct comparison of the measured surface water temperature at TNWA and TNWB against the fixed stations is provided in Figure 5.3 and Figure 5.4, respectively. As could already be inferred from the spatial variations shown in Figure 5.2, the agreements are all excellent.
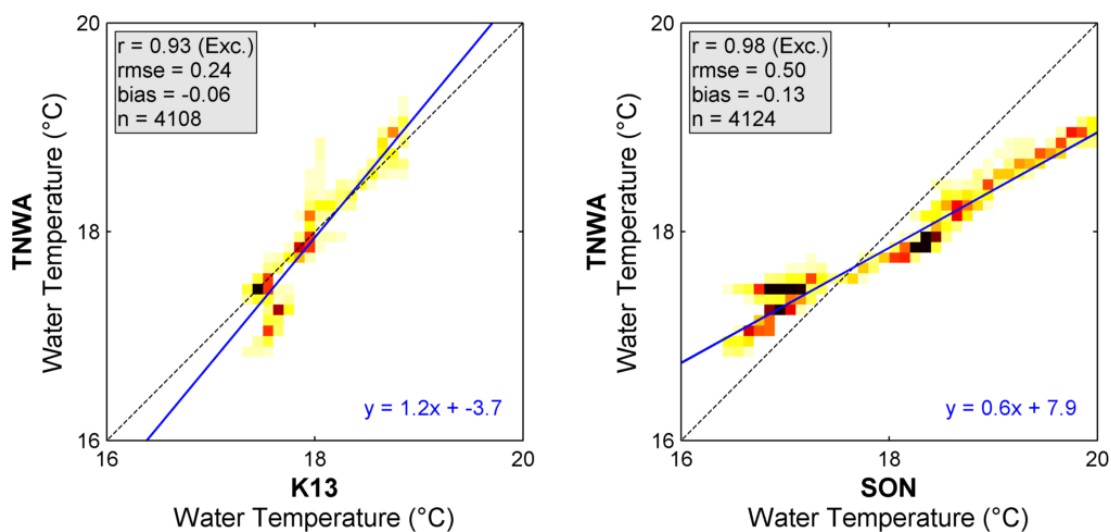
Figure 5.3: *Surface water temperature comparison at TNWA (data from September 2019).*
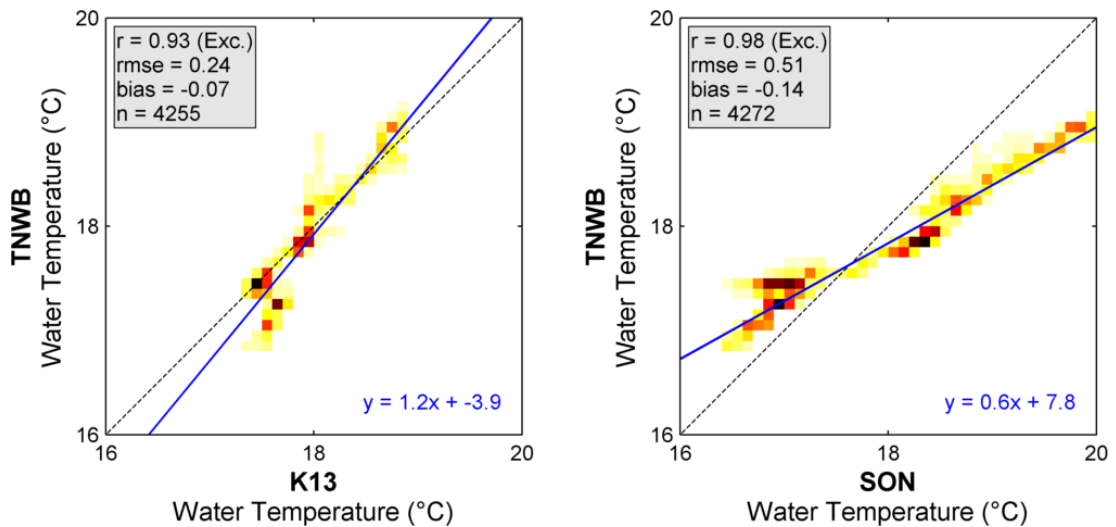
Figure 5.4: *Surface water temperature comparison at TNWB (data from September 2019).*

5.2.2 Air Temperature

A timeseries and a direct comparison between the measured air temperature at TNW and at BG is given in Figure 5.5 and Figure 5.6, respectively. Note that the coarseness of the BG timeseries is due to the 1 °C discretization of the available raw measurements. The figures show a good agreement between the data, with the warmer peak air temperatures being observed at BG.
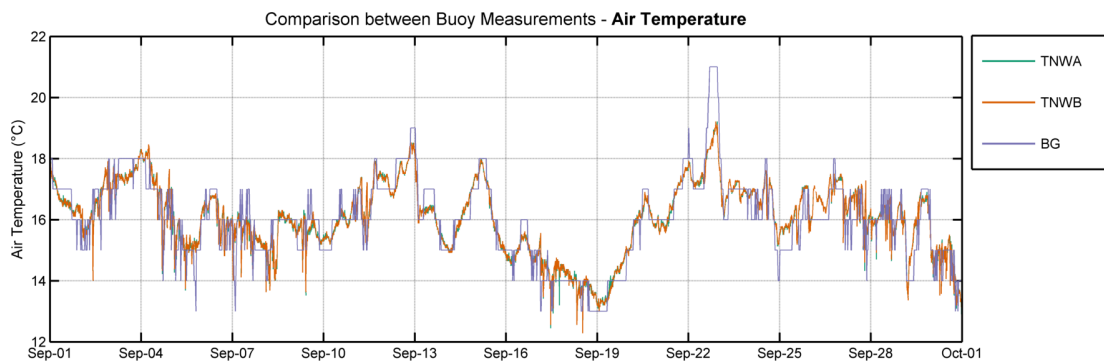
Figure 5.5: *Air temperature measurements from all locations (data from September 2019).*
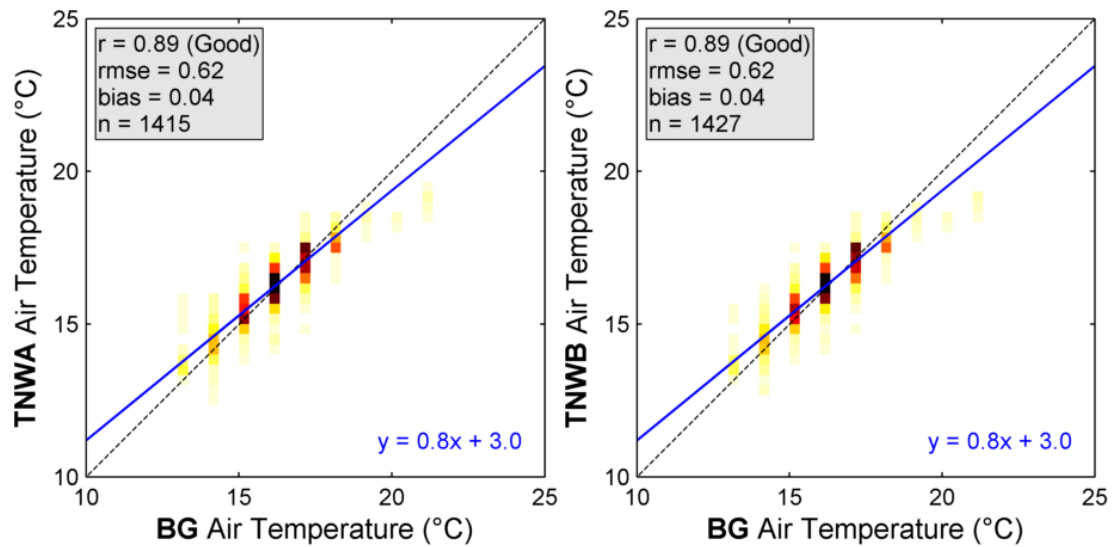
Figure 5.6: *Air temperature comparison at TNWA (left panel) and TNWB (rigth panel). Data from September 2019.*

5.3 Conclusions

The validation of the temperature data shows that there is a general agreement between TNW temperature observations and those from nearby stations.

6 Air Pressure

6.1 Overview

An overview of the available air pressure measurements (e.g. TNWA, TNWB, L91, F161, K13, and F3) is shown in Figure 6.1. The signals from TNW, F3 and F161 show near-identical variations in time, as expected, given their proximity with respect to macro-atmospheric forcings. Furthermore, there is most of the time a gradient between the pressures at the southerner K13 and L91 locations and those in the TNW region. These offsets between the K13 and L91 data and the data from the other stations are not as expect and can be seen as an indication of quality issues in the K13 and the L19 data, but it could not be verified.
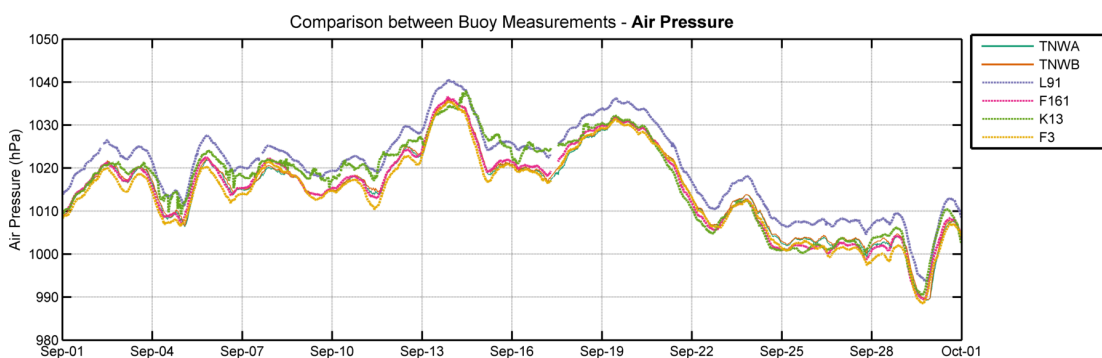
Figure 6.1: Air pressure measurements from all locations.

6.2 Validation

A direct comparison of the measured air pressure at TNWA and TNWB against those of the fixed stations is given in Figure 6.2 and Figure 6.3, respectively. As could already be inferred from the variations shown in Figure 6.1, the agreements are all excellent, but there are large biases between the TNW and the L91 and K13 data.
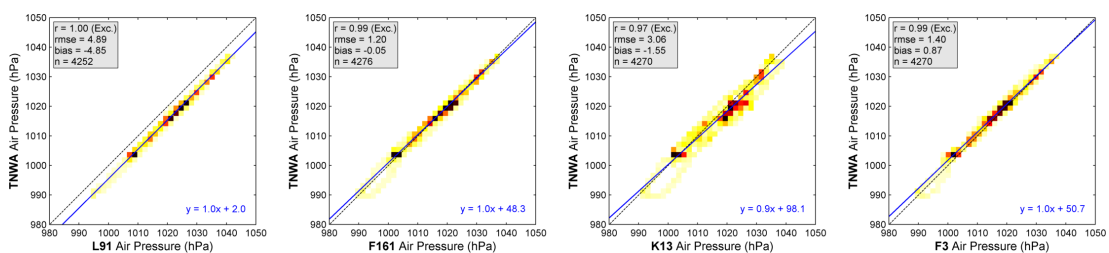
Figure 6.2: Air pressure comparison at TNWA (data from September 2019).
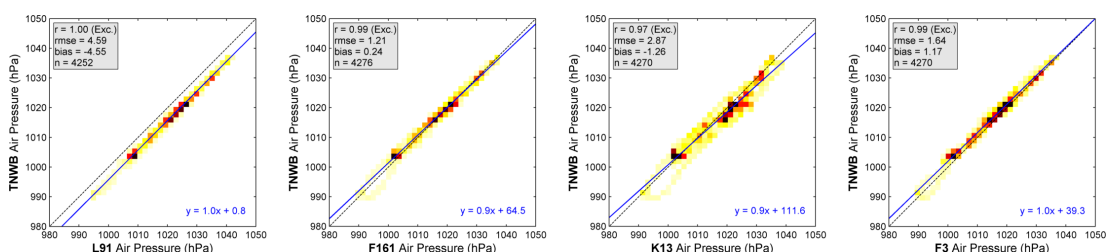
Figure 6.3: Air pressure comparison at TNWB (data from September 2019).

6.3 Conclusions

The validation of the air pressure data shows, as expected given their proximity in terms of macro-atmospheric forcings, an excellent agreement between the TNW observations and those from the fixed stations.

7 Currents

7.1 Ten Noorden van de Waddeneilanden description and intercomparison

The current speed and direction are measured at depths 3 to 38 m with a spacing of 1 m at TNWA and TNWB. Given that the observations close to the bottom are of lower quality and not always available due to the water level variations, in this report we only consider the current velocity data down to a depth of 33 m.

To get a full overview of the data two movies were created with the time evolution of vertical current profiles at TNWA (see here) and TNWB (see here).

Figure 7.1 shows the timeseries of the observed surface (3 m) current speeds, with the corresponding roses being given in Figure 7.2. Figures 7.3 and 7.4 show the observed current speeds and directions, respectively, as a function of depth. As can be seen in the figures, the currents in TNW are predominantly tidally driven, with an alignment close to East-West and with the stronger currents being towards the East.
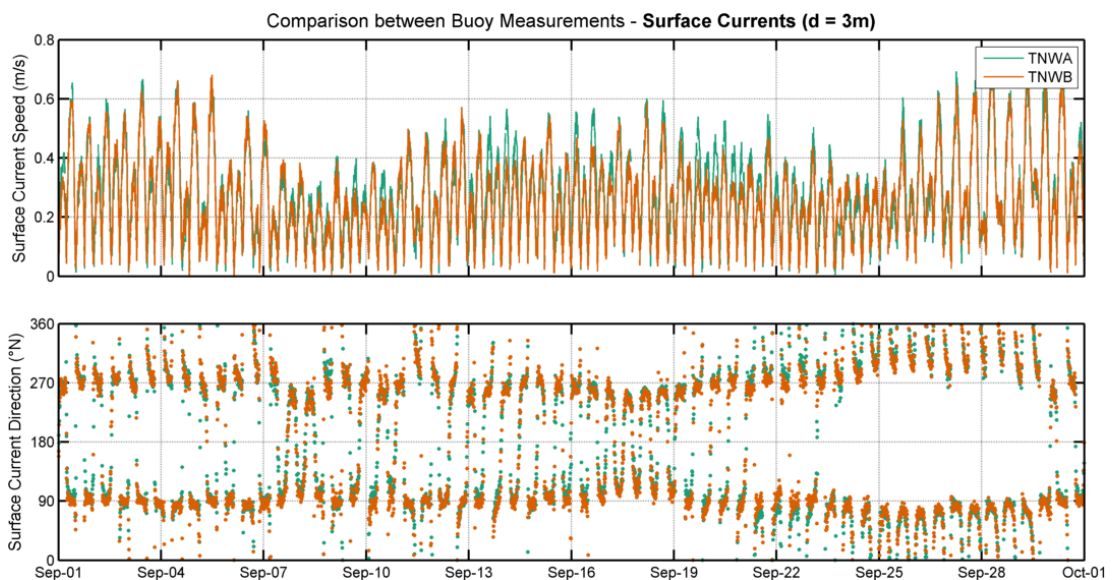
Figure 7.1: *Surface currents at each buoy. Left panels: Timeseries. The oceanographic convention is used for the current directions, so all current directions are going to, clockwise from North.*

Deltares

Comparison between Buoy Measurements - **Surface Currents (d = 3m)**

TNWA

TNWB
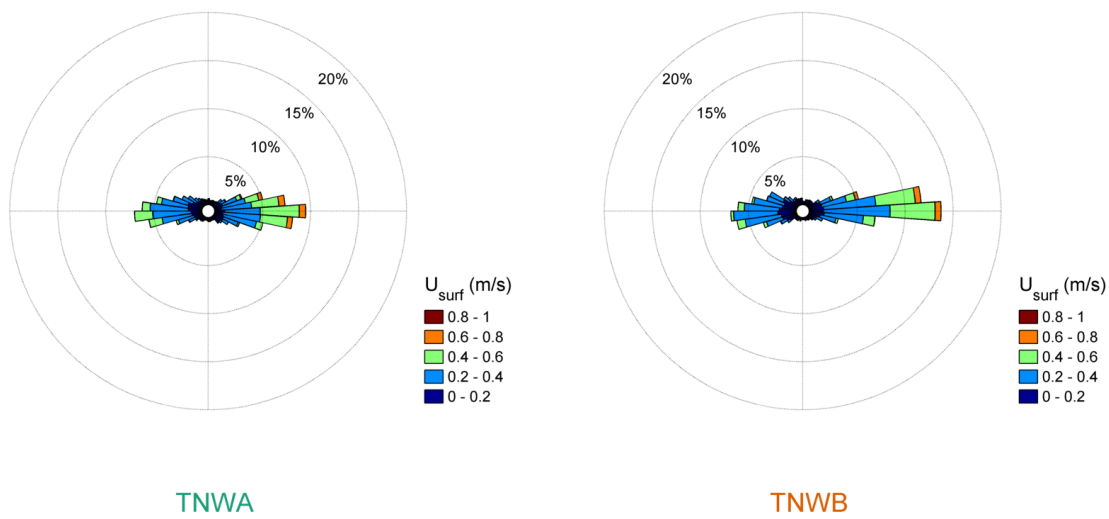
Figure 7.2: *Surface (3 m) current roses (bin width 8°) at each buoy (data from September 2019). The current direction is the direction the piles point to away from the centre of the rose.*
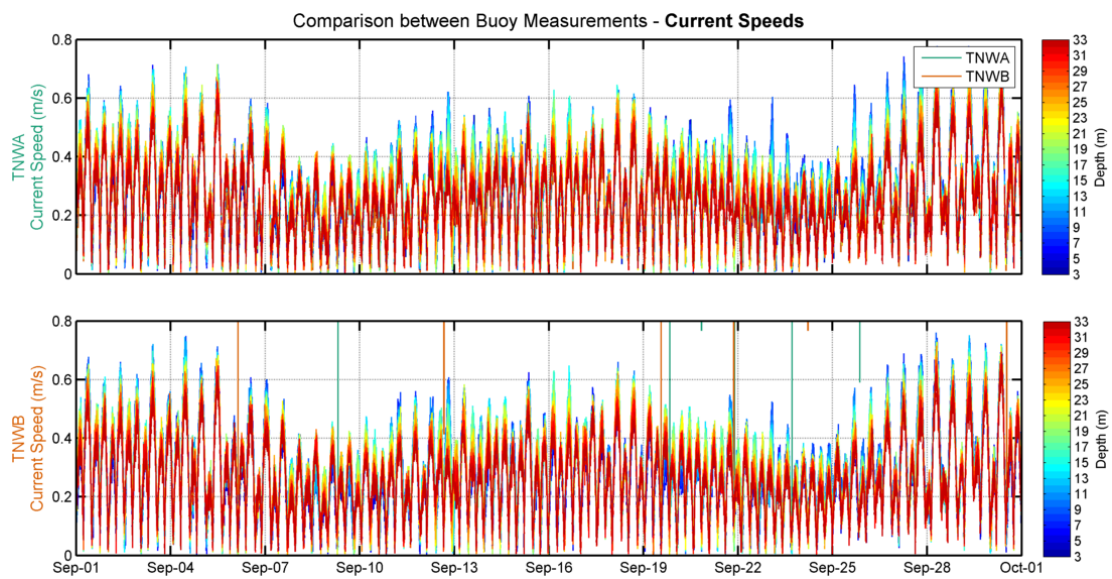
Figure 7.3: *Current speeds (by depth) at each buoy. Left panels: Timeseries.*
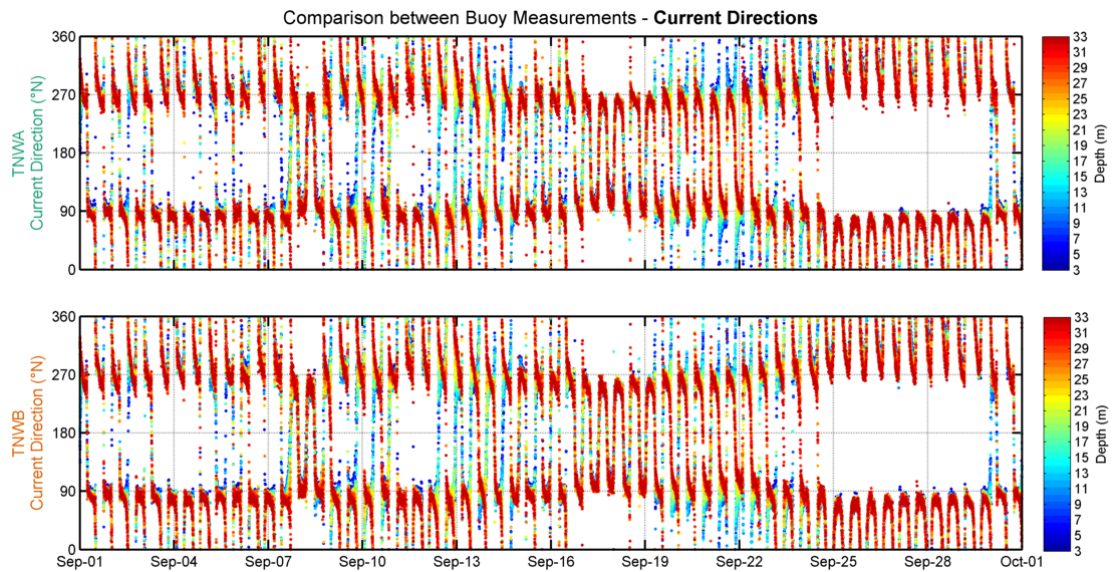
Figure 7.4: *Current directions (by depth) at each buoy (from September 2019). Left panels: Timeseries. The oceanographic convention is used for the current directions, so all current directions are going to clockwise from North.*

Figure 7.5 shows all observed vertical current profiles (grey lines) and the mean profile (red line). Note that, due to the water level variations, the distance between the deepest measuring level and the bottom varies and this leads to a less reliable description of the profile close to the bed using the relative current velocity approach we have applied to compute the profile. Nevertheless, the shown mean profile of TNWA and TNWB observations appears realistic and show, as could already be seen in the figures above, and increase in the current speed from the surface down to a depth of about 6 m and then a steady decrease with depth.
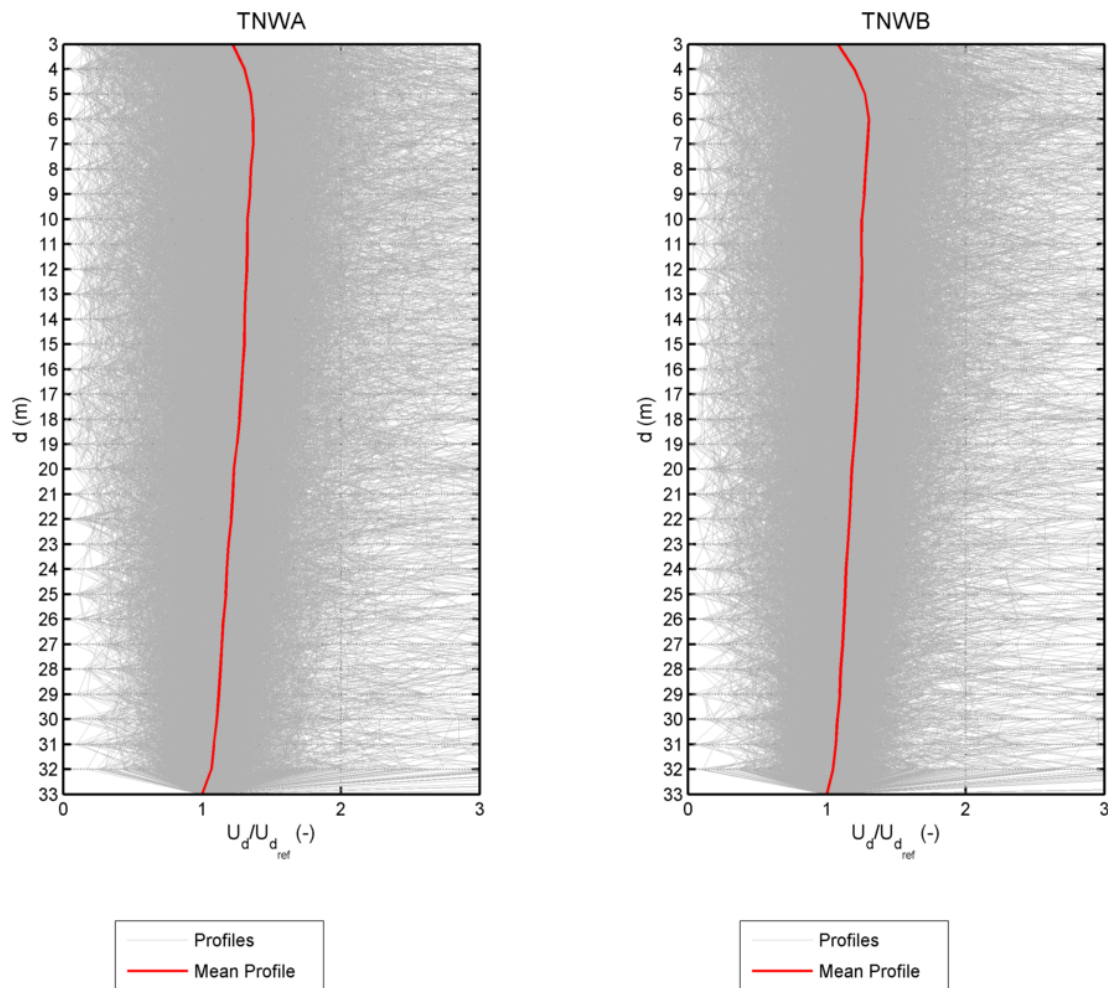
Figure 7.5: *Normalized current speed vertical profiles (from September 2019). The x-axis has a fixed lower limit of 0 and upper limit of 3 for readability.*

In order to further quantify the differences between the currents observed by two buoys, the slope, bias, correlations and square correlations between the TNWA and TNWB current speed observations at all depths and the bias, correlations and square correlations between the TNWA and TNWB current direction observations at all depths have been computed and are given in Table 7.1. The correspondence between the data is excellent in terms of current speed and reasonable to good in terms of current direction. The lower current direction correlations can to a large extent be explained by the nature and variability of the current direction signal. Due to the rotating nature of the currents, especially when they rapidly rotate towards offshore (directions close to 350) the timing can be off. This occurs, however, during short time periods and mostly when the current speeds are low. To demonstrate this further, Table 7.2 shows the current direction statistics computed considering only current speeds above 0.1 m/s. As can be seen in the table, the correspondence between the current direction data is then good to excellent.

Table 7.1: *Statistical comparison between LiDAR buoy current measurements with depth.*

Depth (m)	Current Speed					Current Direction			
	r^2 (-)	r (-)	Bias (m/s)	Symm. Slope (-)	n (-)	r^2 (-)	r (-)	Bias (°N)	n (-)
3	0.86	0.93	-0.02	0.94	4164	0.51	0.71	-2.3	4164
4	0.87	0.93	-0.01	0.96	4164	0.63	0.79	-1.8	4164
5	0.89	0.94	-0.01	0.98	4164	0.67	0.82	-1.7	4164
6	0.90	0.95	-0.00	0.99	4162	0.69	0.83	-1.9	4162
7	0.91	0.95	-0.00	0.99	4164	0.66	0.81	-2.0	4164
8	0.91	0.95	-0.00	0.99	4164	0.67	0.82	-2.4	4164
9	0.91	0.95	-0.00	0.99	4164	0.69	0.83	-3.0	4164
10	0.91	0.95	-0.00	0.99	4164	0.67	0.82	-3.0	4164
11	0.92	0.96	-0.01	0.99	4164	0.65	0.81	-2.7	4164
12	0.92	0.96	-0.00	1.00	4164	0.66	0.81	-2.1	4164
13	0.93	0.96	-0.00	1.00	4164	0.71	0.84	-2.0	4164
14	0.93	0.96	-0.00	0.99	4164	0.68	0.82	-2.4	4164
15	0.93	0.96	-0.00	1.00	4164	0.64	0.80	-2.0	4164
16	0.93	0.96	0.00	1.00	4164	0.64	0.80	-2.3	4164
17	0.93	0.96	-0.00	1.00	4163	0.64	0.80	-2.5	4163
18	0.93	0.96	0.00	1.00	4164	0.64	0.80	-2.9	4164
19	0.92	0.96	-0.00	1.00	4164	0.60	0.78	-3.4	4164
20	0.93	0.96	0.00	1.00	4164	0.63	0.79	-2.7	4164
21	0.93	0.96	0.00	1.00	4164	0.65	0.81	-2.2	4164
22	0.93	0.96	0.00	1.00	4164	0.65	0.80	-2.9	4164
23	0.93	0.96	0.00	1.00	4164	0.67	0.82	-2.8	4164
24	0.93	0.96	0.00	1.00	4164	0.65	0.81	-3.2	4164
25	0.92	0.96	0.00	1.01	4164	0.67	0.82	-2.9	4164
26	0.92	0.96	0.00	1.01	4164	0.70	0.84	-3.7	4164
27	0.92	0.96	0.00	1.01	4164	0.67	0.82	-3.5	4164
28	0.92	0.96	0.00	1.01	4164	0.71	0.84	-3.4	4164
29	0.92	0.96	0.00	1.01	4164	0.71	0.84	-3.2	4164
30	0.91	0.96	0.00	1.01	4164	0.74	0.86	-3.5	4164
31	0.91	0.95	0.00	1.01	4164	0.72	0.85	-3.4	4164
32	0.90	0.95	0.00	1.01	4164	0.72	0.85	-4.0	4164
33	0.88	0.94	0.01	1.03	4163	0.68	0.82	-3.4	4163

Table 7.2: *Statistical comparisons, with depth and considering only speeds above 0.1 m/s, between LiDAR buoy current direction measurements, .*

Depth (m)	Current Direction			
	r^2 (-)	r (-)	Bias (°N)	n (-)
3	0.68	0.82	-2.5	3515
4	0.79	0.89	-2.0	3649
5	0.80	0.89	-1.9	3709
6	0.81	0.90	-2.0	3722
7	0.82	0.91	-2.4	3738
8	0.83	0.91	-2.9	3717
9	0.82	0.91	-3.3	3716
10	0.82	0.90	-3.4	3699
11	0.81	0.90	-2.9	3682
12	0.82	0.90	-2.5	3671
13	0.82	0.91	-2.4	3669
14	0.82	0.91	-2.5	3670
15	0.81	0.90	-2.6	3660
16	0.82	0.90	-2.4	3658
17	0.80	0.89	-2.4	3655
18	0.81	0.90	-2.6	3652
19	0.78	0.89	-2.9	3651
20	0.81	0.90	-2.6	3634
21	0.80	0.89	-2.7	3634
22	0.81	0.90	-2.9	3624
23	0.80	0.90	-3.0	3629
24	0.82	0.90	-2.9	3620
25	0.81	0.90	-3.0	3632
26	0.82	0.91	-3.3	3632
27	0.83	0.91	-3.2	3639
28	0.84	0.91	-3.1	3642
29	0.85	0.92	-3.2	3638
30	0.85	0.92	-3.3	3640
31	0.84	0.92	-3.2	3645
32	0.83	0.91	-3.5	3631
33	0.80	0.89	-3.2	3621

7.2 Validation

The validation of the measured currents at the TNW buoys is completed with data from Deltares 3D Dutch Continental Shelf Model-Flexible Mesh (3D DCSM-FM) described in the following and which has been run purposely for this validation.

7.2.1 Model description

3D DCSM-FM covers the northwest European continental shelf, specifically the area between 15°W to 13°E and 43°N to 64°N, and includes the North Sea and adjacent shallow seas and estuaries such as the Wadden Sea and the Eastern and Western Scheldt. It is loosely based on the two-dimensional operational water level forecasting models of the Netherlands (Zijl *et al.* 2013, 2015), but uses a flexible mesh with resolution increasing with decreasing water depth (Figure 7.6). The smallest cells have a size of 2/3' in east-west direction and 1/2' in north-south direction, which corresponds to 840 m by 930 m in Dutch waters. The optimization methodology is similar to (Zijl *et al.*, 2013), but now excludes bathymetry adjustment. The bathymetry is based on data from EMODnet supplemented with survey data for the Dutch coastal zone (cf. Figure 7.7)). 3D DCSM-FM uses 20 equidistant sigma-layer in the vertical and includes temperature and salinity as state parameters. At the lateral open boundaries water levels consisting of a tide and surge component are provided. For the tide 33 harmonic constituents from the global tide model FES2012 were used, while for the surge an Inverse Barometer Correction is applied (Zijl *et al.*, 2013). The model includes river discharges, while meteorological forcing in terms of atmospheric wind, mean level pressure, air temperature, cloud cover and dew point temperature are obtained from the KNMI operational Numerical Weather Prediction model Hirlam7.2. (Zijl and Veenstra, 2018) provides further details on the set-up and validation of 3D DCSM-FM .
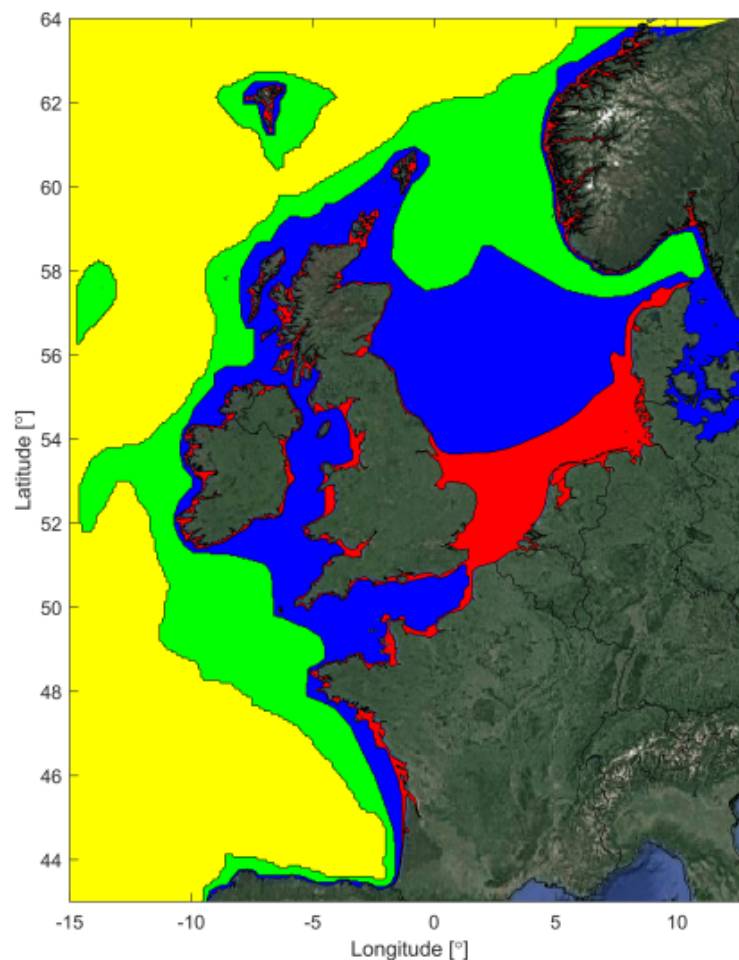
Figure 7.6: *Overview of the 3D DCSM-FM model network with the colors indicating the grid size (yellow: ≈ 4 nm; green: ≈ 2 nm; blue: ≈ 1 nm; red: ≈ 0.5 nm).*
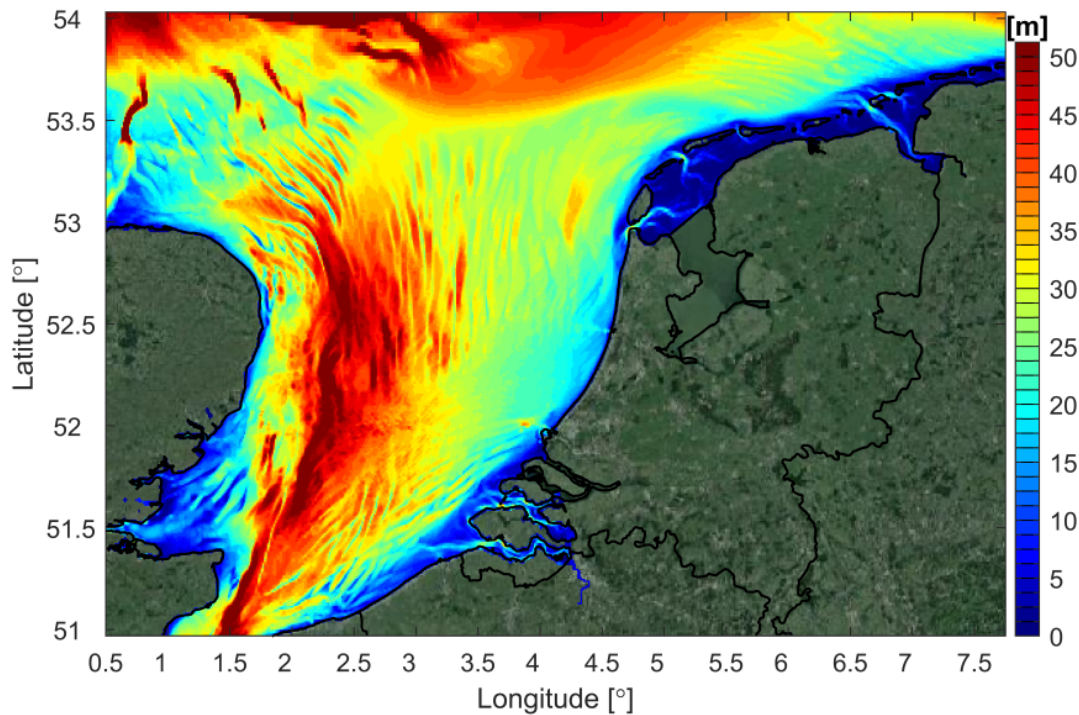
Figure 7.7: *3D DCSM-FM model bathymetry in the southern North Sea (depths relative to MSL; source: EMODnet).*

7.2.2 Model results in Ten Noorden van de Waddeneilanden

The resolution of 3D DCSM-FM in the area of the buoys is about 900 m x 900 m and so the bottom schematization of the model does not fully describe the very fine-scale bottom variations in the area (cf. Figure 1.1). Therefore, the model results are expected to vary more smoothly than the true current variations between the two buoy locations.

Table 7.3 shows the slopes, biases and correlations between the current speed model results at TNWA and TNWB and the correlations and biases between the current direction model results at TNWA and TNWB considering the same depth levels and timestamps as those of the buoy observations given in Table 7.1. Note that the model output at TNWA and TNWB is due to the resolution of the model from adjacent grid points. As expected, the agreement between the data is excellent both in terms of current speed and direction. Note that although the correlations between the directions are lower than those between the speeds, they are still much higher than those obtained between the observed current directions, since the model is not affected in the same way as the buoy by the rapid changes in current direction. Furthermore, the observations show a bias between the current direction at both locations (cf. Table 7.1 and Table 7.2) which is not present in the model results. This is in our opinion again no indication of problems in the observations, but because the model cannot fully describe these local variations in current direction.

Table 7.3: *Statistical comparison between the 3D DCSM-FM results at the buoy locations and at the timestamps at which the buoy data are valid with depth.*

Depth (m)	Current Speed				Current Direction		
	r (-)	Bias (m/s)	Symm. Slope (-)	n (-)	r (-)	Bias (°N)	n (-)
3	1.00	-0.00	0.99	4164	0.99	0.2	4164
4	1.00	-0.00	0.99	4164	0.99	0.1	4164
5	1.00	-0.00	0.99	4164	0.99	0.1	4164
6	1.00	-0.00	0.99	4162	0.98	0.0	4162
7	1.00	-0.00	0.99	4164	0.98	0.0	4164
8	1.00	-0.00	0.99	4164	0.99	-0.0	4164
9	1.00	-0.00	0.99	4164	0.99	-0.1	4164
10	1.00	-0.00	0.99	4164	0.99	0.0	4164
11	1.00	-0.00	0.99	4164	0.99	0.0	4164
12	1.00	-0.00	0.99	4164	0.99	0.0	4164
13	1.00	-0.00	0.99	4164	0.99	0.0	4164
14	1.00	-0.00	0.99	4164	0.98	0.0	4164
15	1.00	-0.00	0.99	4164	0.98	0.0	4164
16	1.00	-0.00	0.99	4164	0.99	0.1	4164
17	1.00	-0.00	0.99	4163	0.99	0.0	4163
18	1.00	-0.00	0.99	4164	0.99	0.2	4164
19	1.00	-0.00	0.99	4164	0.99	0.1	4164
20	1.00	-0.00	0.99	4164	0.99	0.2	4164
21	1.00	-0.00	1.00	4164	0.99	0.1	4164
22	1.00	-0.00	1.00	4164	0.99	0.2	4164
23	1.00	-0.00	1.00	4164	0.99	0.3	4164
24	1.00	-0.00	1.00	4164	0.99	0.3	4164
25	1.00	-0.00	1.00	4164	0.99	0.3	4164
26	1.00	-0.00	1.00	4164	0.99	0.3	4164
27	1.00	-0.00	1.00	4164	0.99	0.3	4164
28	1.00	-0.00	1.00	4164	0.99	0.3	4164
29	1.00	-0.00	1.00	4164	0.99	0.4	4164
30	1.00	-0.00	1.00	4164	0.99	0.4	4164
31	1.00	-0.00	1.00	4164	0.99	0.4	4164
32	1.00	-0.00	1.00	4164	0.99	0.4	4164
33	1.00	-0.00	1.00	4163	0.99	0.4	4163

7.2.3 Ten Noorden van de Waddeneilanden Buoy TNWA

A direct comparison between the 3D DCSM-FM surface current (d = 3 m) at TNWA and the buoy observations is given in Figure 7.8 in terms of timeseries and Figure 7.9 in terms of roses. The same comparisons are shown in Figure 7.10 in terms of timeseries and Figure 7.11 in terms of roses for the current at 23 m (about 60% down the water column). At both levels the agreements are good in terms of current speed and poor in terms of current direction. Furthermore, the roses show more directional spreading in the observations and a larger west-east current asymmetry, with a higher predominance of currents towards the East in the observations. Table 7.4 shows the error statistics between the current speed and direction of the model at TNWA and the TNWA data at the observed levels from a depth of 3 m to 33 m. In terms of current speed (direction) the agreements are good (poor) at all levels.

Figure 7.8: *Surface (d=3 m) current comparison at TNWA (data from September 2019).*

Figure 7.9: *Buoy and 3D DCSM-FM roses (bin width 8°) of the surface (3 m) current velocity at TNWA (data from September 2019. The current direction is the direction the piles point to away from the centre of the rose.*

Figure 7.10: *Current comparison at depth of 23 m TNWA (data from September 2019.*

TNWA comparison between buoy and 3D DCSM-FM currents (d = 23 m)
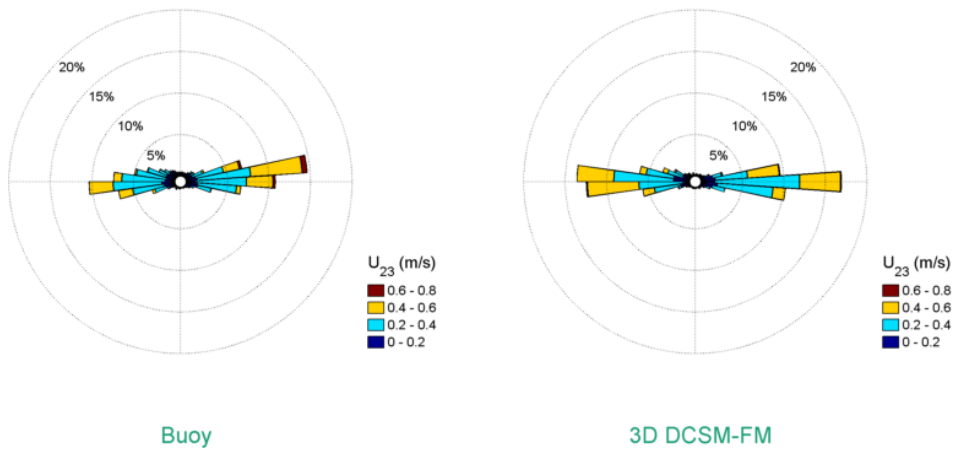
Buoy

3D DCSM-FM

Figure 7.11: *Buoy and 3D DCSM-FM roses (bin width 8°) of the 23 m current velocity at TNWA (data from September 2019). The current direction is the direction the piles point to away from the centre of the rose.*

Table 7.4: *Statistical comparison between the 3D DCSM-FM results with TNWA with depth.*

Depth (m)	Current Speed				Current Direction		
	r (-)	Bias (m/s)	Symm. Slope (-)	n (-)	r (-)	Bias (°N)	n (-)
3	0.88	-0.04	0.89	4166	0.61	5.0	4166
4	0.87	-0.02	0.94	4166	0.62	1.1	4166
5	0.87	-0.01	0.96	4166	0.63	0.3	4166
6	0.86	-0.01	0.97	4166	0.62	-0.5	4166
7	0.87	-0.01	0.97	4166	0.61	-0.4	4166
8	0.87	-0.01	0.96	4166	0.60	-0.4	4166
9	0.86	-0.01	0.96	4166	0.61	0.3	4166
10	0.86	-0.01	0.95	4166	0.59	-0.0	4166
11	0.86	-0.01	0.96	4166	0.60	0.1	4166
12	0.87	-0.01	0.97	4166	0.56	-0.7	4166
13	0.88	-0.01	0.97	4166	0.56	-0.9	4166
14	0.88	-0.01	0.96	4166	0.55	-0.9	4166
15	0.87	-0.01	0.97	4166	0.54	-0.7	4166
16	0.87	-0.01	0.96	4166	0.51	-1.1	4166
17	0.86	-0.01	0.97	4166	0.52	-0.1	4166
18	0.86	-0.01	0.96	4166	0.53	0.8	4166
19	0.85	-0.01	0.96	4166	0.52	1.1	4166
20	0.86	-0.01	0.95	4166	0.55	1.6	4166
21	0.85	-0.01	0.95	4166	0.55	1.3	4166
22	0.86	-0.01	0.95	4166	0.57	2.3	4166
23	0.85	-0.01	0.95	4166	0.59	2.2	4166
24	0.85	-0.01	0.95	4166	0.61	2.5	4166
25	0.84	-0.01	0.96	4166	0.60	3.8	4166
26	0.84	-0.01	0.95	4166	0.61	3.6	4166
27	0.83	-0.01	0.96	4166	0.59	4.1	4166
28	0.83	-0.01	0.95	4166	0.60	3.7	4166
29	0.82	-0.01	0.95	4166	0.59	3.8	4166
30	0.83	-0.02	0.94	4166	0.59	3.8	4166
31	0.82	-0.01	0.95	4166	0.59	4.4	4166
32	0.81	-0.02	0.93	4166	0.58	3.4	4166
33	0.80	-0.02	0.93	4166	0.57	3.7	4166

7.2.4 Ten Noorden van de Waddeneilanden Buoy TNWB

A direct comparison between the 3D DCSM-FM surface current (d = 3 m) at TNWB and the buoy observations is given in Figure 7.12 in terms of timeseries and Figure 7.13 in terms of roses. The same comparisons are shown in Figure 7.14 in terms of timeseries and Figure 7.15 in terms of roses for the current at 23 m (about 60% down the water column). As was the case for TNWA, at both levels the agreements are good in terms of current speed and poor in terms of current direction, with the misalignments occurring mostly by low current speeds. Also, although the misalignments occur mostly by low current speeds, the spreading in the observed current directions is wider and with a larger west-east current asymmetry. Table 7.4 shows the error statistics between the current speed and direction of the model at TNWB and the TNWB data at the observed levels from a depth of 3 m to 33 m. Again as was the case for TNWA, in terms of current speed (direction) the agreements are good (poor).
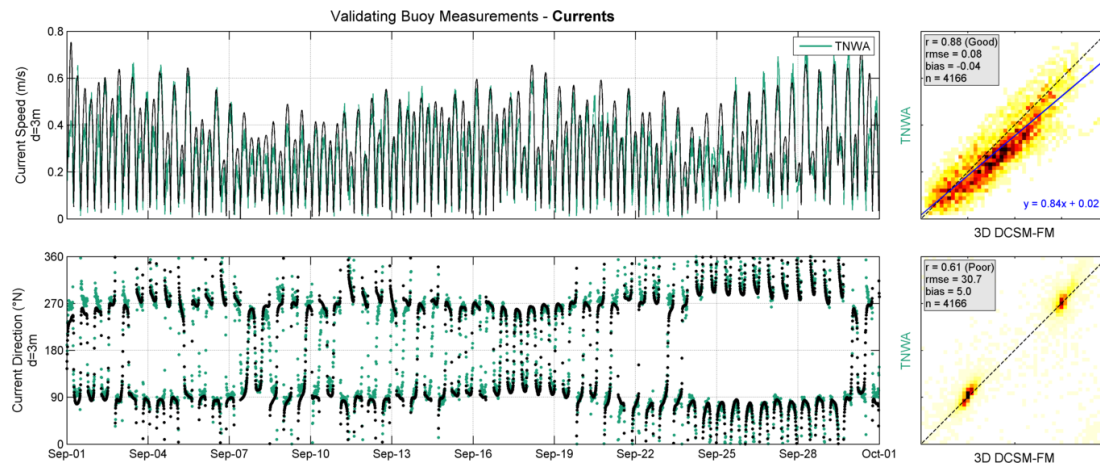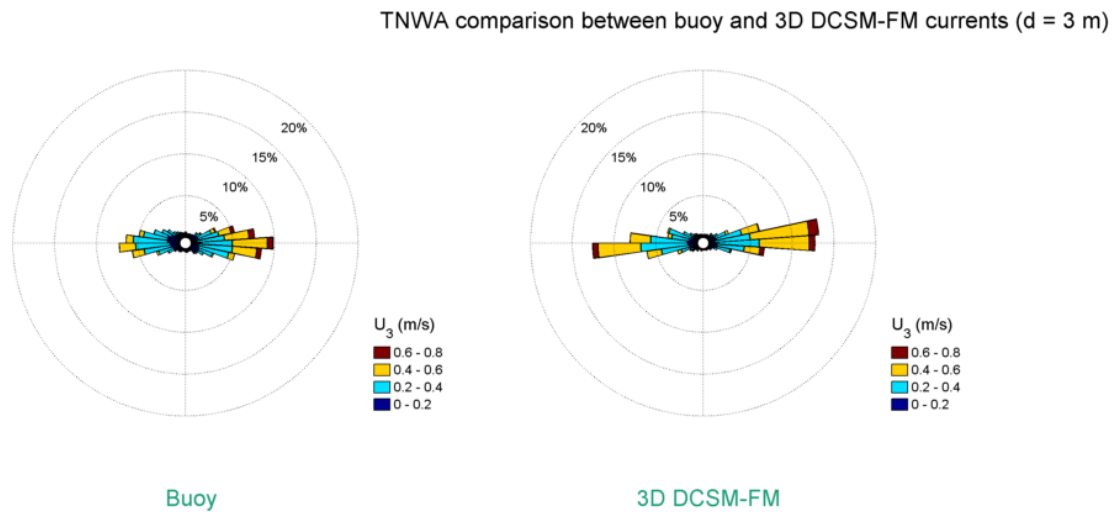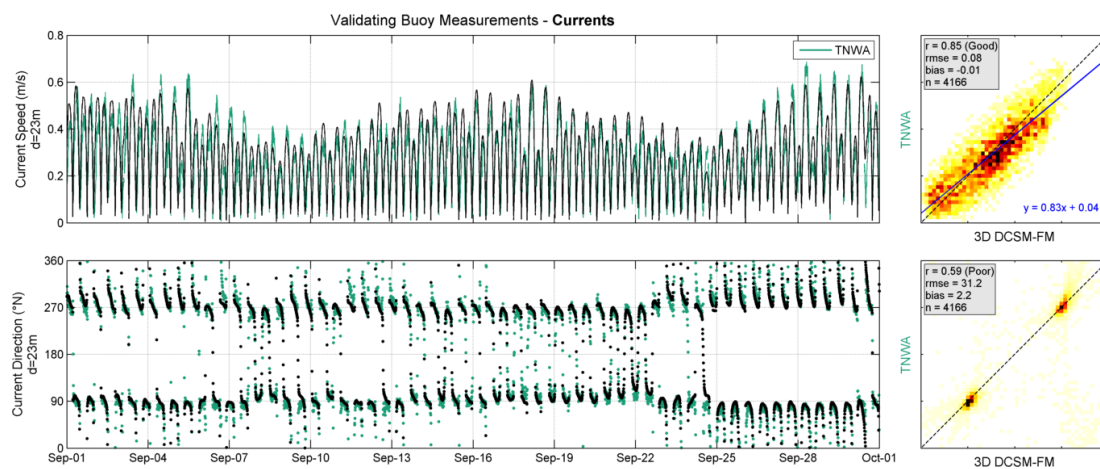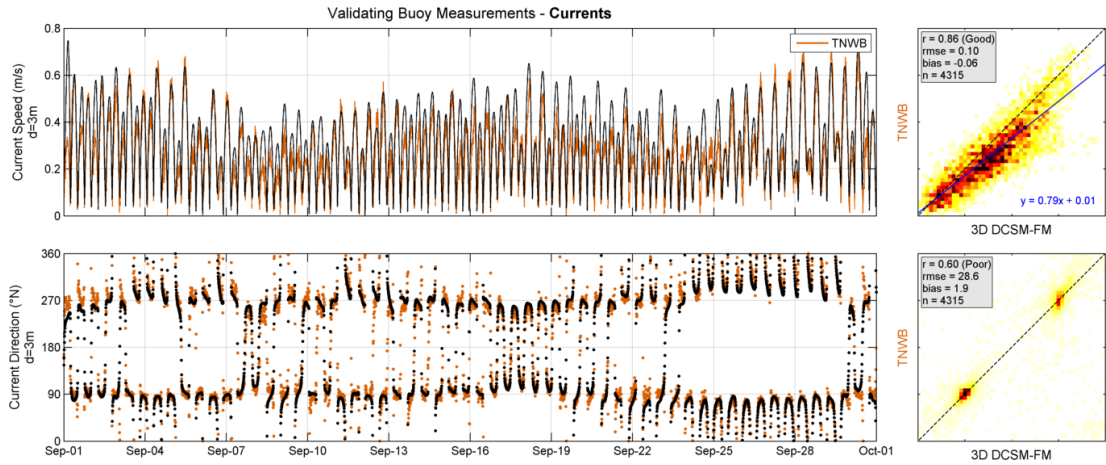
Figure 7.12: *Surface (d = 3 m) current comparison at TNWB (data from September 2019).*
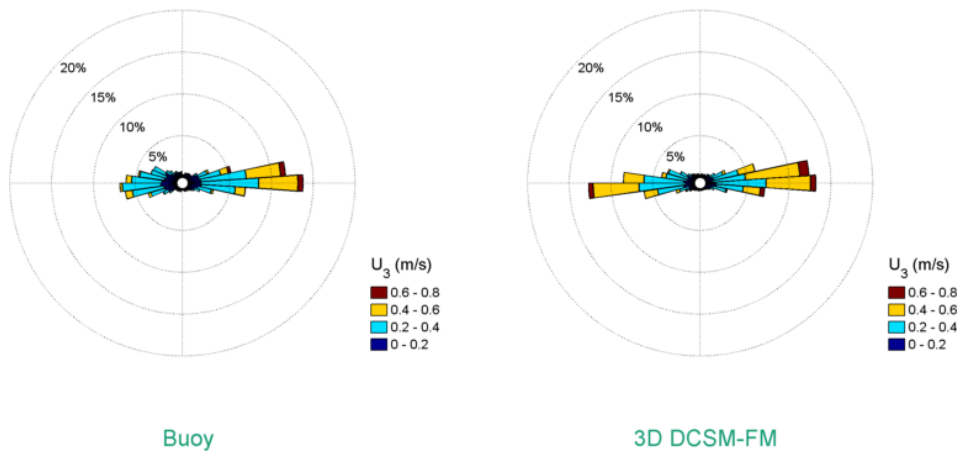
Figure 7.13: *Buoy and 3D DCSM-FM roses (bin width 8°) of the surface (d = 3 m) current velocity at TNWB (data from September 2019). The current direction is the direction the piles point to away from the centre of the rose.*

Figure 7.14: *Current comparison at a depth of 23 m TNWB.*

Figure 7.15: *Buoy and 3D DCSM-FM roses (bin width 8°) of the 23 m current velocity at TNWB (data from September 2019) The current direction is the direction the piles point to away from the centre of the rose.*

Table 7.5: *Statistical comparison between the 3D DCSM-FM results with TNWB with depth.*

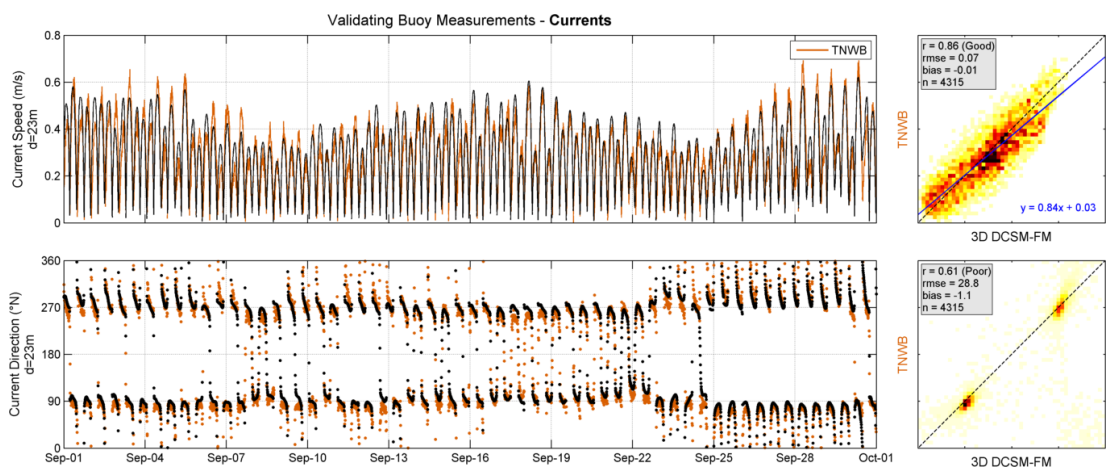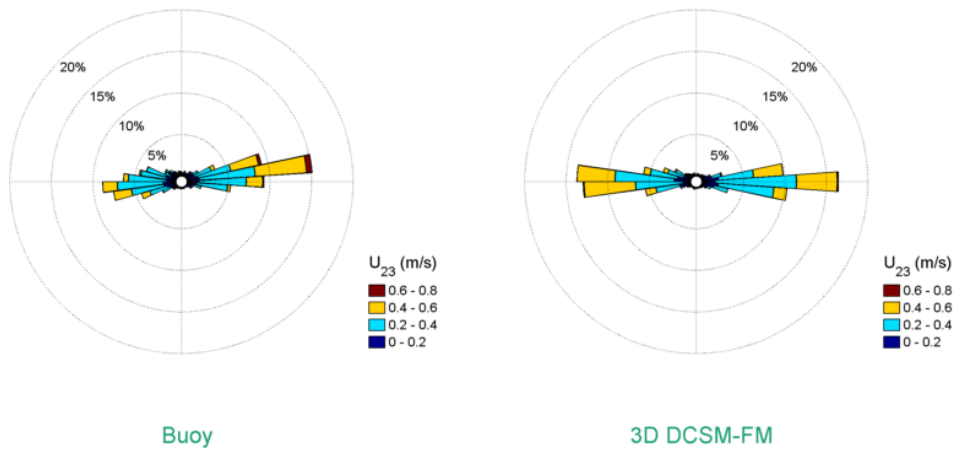| Depth (m)	Current Speed				Current Direction		
	r (-)	Bias (m/s)	Symm. Slope (-)	n (-)	r (-)	Bias (°N)	n (-)
3	0.86	-0.06	0.84	4315	0.60	1.9	4315
4	0.83	-0.03	0.91	4315	0.63	-0.9	4315
5	0.84	-0.02	0.95	4315	0.65	-1.4	4315
6	0.84	-0.01	0.96	4313	0.61	-1.5	4313
7	0.85	-0.01	0.96	4315	0.63	-1.6	4315
8	0.85	-0.01	0.96	4315	0.59	-2.4	4315
9	0.85	-0.01	0.95	4315	0.59	-2.1	4315
10	0.85	-0.02	0.95	4315	0.54	-3.1	4315
11	0.86	-0.01	0.95	4315	0.57	-2.3	4315
12	0.89	-0.01	0.97	4315	0.54	-2.6	4315
13	0.89	-0.01	0.97	4315	0.55	-2.2	4315
14	0.89	-0.01	0.96	4315	0.52	-2.7	4315
15	0.89	-0.01	0.97	4315	0.53	-3.0	4315
16	0.88	-0.01	0.97	4315	0.51	-2.4	4315
17	0.88	-0.01	0.97	4314	0.51	-1.8	4314
18	0.88	-0.01	0.96	4315	0.52	-1.6	4315
19	0.87	-0.01	0.97	4315	0.55	-1.4	4315
20	0.87	-0.01	0.96	4315	0.54	-1.4	4315
21	0.87	-0.01	0.96	4315	0.57	-1.3	4315
22	0.87	-0.01	0.96	4315	0.60	-1.0	4315
23	0.86	-0.01	0.96	4315	0.61	-1.1	4315
24	0.87	-0.01	0.96	4315	0.63	-0.8	4315
25	0.86	-0.01	0.96	4315	0.62	-0.4	4315
26	0.86	-0.01	0.96	4315	0.62	-0.4	4315
27	0.85	-0.01	0.97	4315	0.59	0.1	4315
28	0.85	-0.01	0.96	4315	0.60	-0.2	4315
29	0.85	-0.01	0.97	4315	0.57	0.3	4315
30	0.84	-0.01	0.95	4315	0.60	0.1	4315
31	0.84	-0.01	0.96	4315	0.57	-0.0	4315
32	0.83	-0.01	0.95	4315	0.58	-0.5	4315
33	0.82	-0.01	0.96	4314	0.58	-0.4	4314

7.3 Conclusions

As shown above, the agreement between the current speed observations from both buoys and from each buoy with model results is high. The obtained relatively lower correlations in the current direction are not considered to be due to lack of accuracy in the current direction observations, but model resolution effects and the effect of the nature and variability of the current direction signal on the buoy observations. The found general agreement between the buoy and model data at the two locations, testify the quality of both the model results and the observations.

8 Final remarks

Two *SEAWATCH Wind LiDAR Buoys*, TNWA and TNWB, and a bottom mounted sensor close to TNWB, have been deployed by Fugro at the Ten Noorden van de Waddeneilanden Wind Farm Zone on the 19th of June 2019, with the intention of measuring wind, waves, temperatures, pressures and currents for a period of two years. This report focuses on the validation of the measurements from September 2019.

The validation is performed by comparing the TNWA and TNWB observations against each other and with wind, waves, air and water temperature, air pressure and currents from a variety of reliable sources (anemometer, LiDAR, hydrodynamic model, etc) at reference stations in the North Sea; namely L91, F161, K13, F3, AWG, HG, SON and BG.

The following conclusions ensue from the validation of the data.

- The comparisons between the TNWA and TNWB wind velocities show at all levels and in terms of both wind speed and direction low biases and correlations and slopes close to 1, indicating correct functioning of both LiDARs. Furthermore, there is a poor to reasonable (reasonable to excellent) agreement between the wind speed (direction) observations from TNW and those from the fixed platforms. The found mismatches can be explained by local effects and spatial variations.
- The agreement between the TNWA and TNWB wave parameters is excellent for all parameters, except in terms of peak wave period which is good and mean wave direction of swell which is poor. The poorer agreements are as expected, given that these parameters depend more strongly on the sampling variability (randomness of the sea surface elevation) and discreteness of the wave spectra. The agreement between the wave observations from TNW and from the reference stations is relatively high, especially when considering local refraction and the distances between the stations.
- The validation of the temperature data shows that there is a general agreement between TNW temperature observations and those from nearby stations.
- The validation of the air pressure data shows, as expected given their proximity in terms of macro-atmospheric forcings, an excellent agreement between the TNW observations and those from the fixed stations.
- The agreement between the current speed observations and model results is high. There are mismatches between the current directions, which are partly due to the nature and variability of the current direction signal.

The availability of the buoy data is high for all variables except for the LiDAR wind data which is poor, with no data available from the LiDAR at TNWB from 00:10 on the 12th of September, when connection was lost, and many gaps in the TNWA data.

The overall conclusion of the validation is that the TNWA and TNWB datasets are of high quality and trustworthy.

References

DNV-GL, 2019a. *FUGRO SEAWATCH WIND LIDAR BUOY WS 190 PRE-DEPLOYMENT VALIDATION; Assessment of the Fugro Seawatch Wind LiDAR Buoy WS 190 Pre-Deployment Validation at Frøya, Norway*. Tech. Rep. 10129033-R-10, Rev. A, 2019-06-25, DNV-GL.

DNV-GL, 2019b. *FUGRO SEAWATCH WIND LIDAR BUOY WS 190 PRE-DEPLOYMENT VALIDATION; Assessment of the Fugro Seawatch Wind LiDAR Buoy WS 191 Pre-Deployment Validation at Frøya, Norway*. Tech. Rep. 10129033-R-11, Rev. A, 2019-06-25, DNV-GL.

Fisher, N. I., 1993. *Statistical analysis of circular data*. Cambridge Univ. Press.

Fisher, N. I. and A. J. Lee, 1983. "A correlation coefficient for circular data." *Biometrika* 70: 327–332.

IEA Wind, 2017. *"18. FLOATING LIDAR SYSTEMS", IEA Wind Expert group report on recommended practices, 1st edition, September 2017*. Tech. rep.

IEC 61400-12-1, 2017. *IEC 61400-12-1 Wind energy generation systems | Part 12-1: Power performance measurements of electricity producing wind turbines . IEC-TC88 Maintenance Team MT12-1 , Edition 2.0 , 3 March 2017*. Tech. rep.

KNMI, 2009. *HiRLAM version H7.2*. Tech. Rep. http://projects.knmi.nl/datacentrum/catalogus/catalogus/content/history/HIRLAM72_eng__151009.pdf, KNMI.

Wieringa, J. and P. Rijkoort, 1983. *Windklimaat van Nederland (in Dutch)*. KNMI (staatsuitgeverij).

Zijl, F., J. Sumihar and M. Verlaan, 2015. "Application of data assimilation for improved operational water level forecasting on the northwest European shelf and North Sea." *Ocean Dynamics* 65 (11).

Zijl, F. and J. Veenstra, 2018. *Setup and validation of 3D DCSM-FM*. Deltares memo 1220339-005-zks-0003.

Zijl, F., M. Verlaan and H. Gerritsen, 2013. "Improved water-level forecasting for the Northwest European Shelf and North Sea through direct modelling of tide, surge and non-linear interaction." *Ocean Dynamics* 63 (7).